Mutations in ACTL6B Cause Neurodevelopmental Deficits and Epilepsy and Lead to Loss of Dendrites in Human Neurons

Scott Bell, Justine Rousseau, Huashan Peng, Zahia Aouabed, Pierre Priam, Jean-Francois Theroux, Malvin Jefri, Arnaud Tanti, Hanrong Wu, Ilaria Kolobova, et al.

Mutations in *ACTL6B* cause neurodevelopmental deficits and epilepsy and lead to loss of dendrites in human neurons

Scott Bell [1,34], Justine Rousseau [2,34], Huashan Peng[1], Zahia Aouabed[1], Pierre Priam[3], Jean-Francois Theroux[1], Malvin Jefri[1], Arnaud Tanti[1], Hanrong Wu[1], Ilaria Kolobova[1], Heika Silviera[1], Karla Manzano-Vargas[1], Sophie Ehresmann[2], Fadi F Hamdan[2], Nuwan Hettige[1], Xin Zhang [1], Lilit Antonyan[1], Christina Nassif[2], Lina Ghaloul-Gonzalez[4], Jessica Sebastian[5], Jerry Vockley[5], Amber G. Begtrup[6], Ingrid M. Wentzensen[6], Amy Crunk[6], Robert D. Nicholls[7], Kristin C Herman[7], Joshua Deignan[8], Walla Al-Hertani[9], Stephanie Efthymiou[10], Vincenzo Salpietro[10], Noriko Miyake[11], Yoshio Makita[12], Naomichi Matsumoto[11], Rune Østern[13], Gunnar Houge[14], Maria Hafström[13], Emily Fassi[15], Henry Houlden[16], Jolien S Klein Wassink-Ruiter[17], Dominic Nelson[18], Amy Goldstein[19], Tabib Dabir[20], Julien van Gils[21], Thomas Bourgeron[21], Richard Delorme[22], Gregory M Cooper[23], Jose E. Martinez[24], Candice R Finnila[25], Lionel Carmant[24], Anne Lortie[25], Renske Oegema[26], Koen van de Gassen[26], Sarju G. Mehta[27], Dagmar Huhle[27], Rami Abou Jamra[28], Sonja Martin[28], Han Brunner [29,30], Dick Lindhout[31], Margaret Au[32], John M Graham Jr[32], Christine Coubes[33], Gustavo Turecki[1], Simon Gravel[17], Naguib Mechawar[1], Elsa Rossignol[2], Jacques L Michaud[2], Julie Lessard[3], Carl Ernst [1,34,*], Philippe M Campeau [2,34,*]

Affiliations

1) Psychiatric Genetics Group, Douglas Hospital Research Institute, McGill University, Montreal, QC, Canada, H4H 1R3
2) CHU-Sainte Justine Research Centre, University of Montreal, Montreal, QC, Canada, H3T 1C5,
3) Institute for Research in Immunology and Cancer (IRIC), University of Montreal, Montreal, Quebec, Canada, H3T 1J4

4) Department of Pediatrics, University of Pittsburgh, Children's Hospital of Pittsburgh of UPMC, Pittsburgh, PA, USA
5) Division of Medical Genetics, University of Pittsburgh, Children's Hospital of Pittsburgh of UPMC, Pittsburgh, PA, USA
6) Gene Dx, Gaithersburg, MD 20877, USA
7) University of California at Davis Medical Center, Section of Medical Genomics, Sacramento, CA, USA 95817
8) Department of Pathology and Laboratory Medicine, David Geffen School of Medicine at UCLA, CA, USA
9) Departments of Medical Genetics and Paediatrics, Cumming School of Medicine, Alberta Children's Hospital and University of Calgary, Calgary, AB T3B 6A8
10) Department of Molecular Neuroscience, UCL Institute of Neurology, Queen Square WC1N 3BG, London, UK
11) Department of Human Genetics, Yokohama City University Graduate School of Medicine, Yokohama 236-0004,Japan
12) Education Center, Asahikawa Medical University, Asahikawa 078-8510, Japan,
13) Department of Medical Genetics, St. Olavs hospital, Trondheim University Hospital, Postbox 3250 Sluppen, NO-7006 Trondheim
14) Department of Medical Genetics, Haukeland University Hospital, 5021 Bergen, Norway
15) Division of Genetics and Genomic Medicine, Department of Pediatrics, Washington University School of Medicine, St. Louis, MO, USA, 63110
16) Department of Molecular Neuroscience, UCL Institute of Neurology, Queen Square WC1N 3BG, London, UK
17) Department of Genetics, University of Groningen and University Medical Center Groningen, 9700 RB Groningen, the Netherlands
18) McGill University, Department of Human Genetics, Montreal, QC, H3G 0B1
19) Division of Child Neurology, Children's Hospital of Pittsburgh, Pittsburgh, Pennsylvania, USA.
20) Northern Ireland Regional Genetics Centre, Belfast Health and Social Care Trust, Belfast City Hospital, Lisburn Road, Belfast BT9 7AB, UK
21) Human Genetics and Cognitive Functions, Institut Pasteur,, 25 Rue du Docteur Roux, Paris, Cedex 15 France
22) Assistance Publique Hôpitaux de Paris (APHP), Robert Debré Hospital, Child and Adolescent Psychiatry Department, Paris, France
23) HudsonAlpha Institute for Biotechnology, Huntsville, AL 35806
24) Children’s Rehabilitation Service, Mobile, AL 36604
25) Department of Neurology, University of Montreal, Montreal, Canada
26) Department of Genetics, University Medical Center Utrecht, 3508 AB Utrecht, the Netherlands.
27) Department of Clinical Genetics, Addenbrookes Hospital, Cambridge CB2 0QQ
28) Institute of Human Genetics, University Medical Center Leipzig, 04103 Leipzig, Germany
29) Department of Human Genetics, Radboud University Medical Center, Donders Institute for Brain, Cognition and Behaviour, Nijmegen, 6500 GA, The Netherlands.
30) Department of Clinical Genetics and School for Oncology & Developmental Biology (GROW), Maastricht University Medical Center, 6202 AZ, Maastricht, The Netherlands.
31) Department of Genetics, University Medical Center Utrecht, Utrecht & Stichting Epilepsie Instellingen Nederland (SEIN), Heemstede, The Netherlands.
32) Medical Genetics, Cedars Sinai Medical Center, Los Angeles CA 90048 USA

33) Service de génétique clinique, Département de génétique médicale, Maladies rares et médecine personnalisée, Centre de Référence Anomalies du développement et Syndromes malformatifs du Sud-Ouest Occitanie Réunion, CHU de Montpellier, 34295 Montpellier cedex 5, France
34) Equally contributing authors

*Corresponding authors: carl.ernst@mcgill.ca; p.campeau@umontreal.ca

Running title (40 characters): Mutations in *ACTL6B* cause neurodevelopmental disorders

Keywords: Intellectual disability, seizure, *ACTL6B*, stem cells, genetic engineering, neurodevelopment

Abstract

We identified individuals with mutations in ACTL6B, a component of the chromatin remodelling machinery including the BAF complex. Ten individuals harbored bi-allelic mutations and presented with global developmental delay, epileptic encephalopathy and spasticity, and ten individuals with de novo heterozygous mutations displayed intellectual disability, ambulation deficits, severe language impairment, hypotonia, Rett-like stereotypies and minor facial dysmorphisms (wide mouth, diastema, bulbous nose). Nine of these ten unrelated individuals had the identical de novo c.1027G>A mutation. Human derived neurons were generated that recaptured *ACTL6B* expression patterns in development from progenitor cell to post-mitotic neuron, validating the use of this cell model. Engineered knock-out of *ACTL6B* in wildtype human neurons resulted in profound deficits in dendrite development, a result recapitulated in two individuals with different bi-allelic mutations, and reversed on clonal genetic repair or exogenous expression of *ACTL6B*. Whole transcriptome analyses and whole genomic profiling of the BAF complex in wildtype and biallelic mutant *ACTL6B* NPCs and neurons revealed increased genomic binding of the BAF complex in *ACTL6B* mutant cells, with corresponding transcriptional changes in several genes including *TPPP* and *FSCN1*, suggesting that altered regulation of some cytoskeletal genes contribute to altered dendrite development. Assessment of bialleic and heterozygous *ACTL6B* mutations on an *ACTL6B* KO human background demonstrated that biallelic mutations mimic engineered deletion deficits while heterozygous mutations do not, suggesting that the former are loss-of-function and the latter are gain-of function. These results reveal a role for *ACTL6B* in neurodevelopment, and implicate another component of chromatin remodelling machinery in brain disease.

Introduction

ACTL6B (MIM: 612458) encodes an actin-related protein (ARP), which are a class of proteins that resemble actin and have roles in chromatin remodelling and histone acetylation[1]. Though ACTL6B, known as BAF53B, may interact with multiple complexes in a particular spatiotemporal order, most investigations have focused on its role in the BAF (BRG1/BRM-Associated Factor), or SWI/SNF complex[2], which serves as an important regulator of gene expression by remodeling nucleosomes in an ATP-dependant fashion[3-5]. In order to regulate different sets of genes during development, BAF subunits can be exchanged with homologous alternatives[3]. One such switch in BAF subunit composition occurs in developing neural cells as they exit the cell cycle. During this time, the neural progenitor specific BAF (npBAF) complex transitions to the neural specific BAF (nBAF) complex through the exchange of several subunits, including BAF53A for its paralog BAF53B[6]. This is partly achieved through increased expression of miR-9* and miR-124 in post mitotic neurons, which repress the expression of the gene that encodes BAF53A, *ACTL6A* (MIM: 604958)[7]. nBAF complexes can bind the transactivator CREST and be recruited to genes crucial for dendritogenesis through interactions mediated by BAF53B[8]. As a result, loss of BAF53B protein levels during neuronal development results in impaired dendritic outgrowth. An *Actl6b* KO mouse has previously been generated, and found to have deficits in dendritic spine and synapse function, leading to impaired long-term memory and poor survival[9].

While different genes that contribute to the BAF complex have been found to be associated with human disease (e.g., Nicolaides-Baraitser syndrome MIM: 601358, *SMARCA2* MIM:600014; Coffin-Siris syndrome MIM: 135900, *ARID1B; MIM:* 614556)[10; 11], *ACTL6B* has not been conclusively reported to have a deleterious role in human neurological diseases. In this study, we identified individuals with neurodevelopmental

disorders with either inherited recessive mutations or dominantly acting *de novo* mutations in *ACTL6B*, and sought to understand how mutations in *ACTL6B* might affect the development of human neurons.

Materials and methods

Description of studied individuals. Individuals had whole exome sequencing as part of local neurodevelopmental studies on developmental delay and intellectual disability, autism or epilepsy (R1, R2a/b, R3a/b, R4, R5, R7, R9, R10, D2, D3, D7, D8). Informed consent for participating in the genetic studies was obtained on protocols approved by institutional review boards of local hospitals. Individuals D1 and D4 were enrolled in the DDD study and provided informed consent for this study. Other individuals had exome sequencing at GeneDx as part of clinical care (individuals R6, R8a/b, D5, D6, D9), and after *ACTL6B* was identified as a candidate gene, provided informed consent for the sharing of photographs or samples as applicable.

Experimental procedures for sequencing. DNA was extracted from peripheral blood from affected individuals and parents using standard protocols. For individuals who had Whole Genome Sequencing (R1, R2a/b, R10), the DNA libraries were prepared by using the Illumina TruSeq DNA PCR-Free kits using the manufacturer's protocol. For individuals who had Whole Exome Sequencing, the exome libraries were prepared using Agilent SureSelect kits (R3ab, R4, R6, R8ab, R9, D1, D2, D4-D9), Roche-NimbleGen EZ exome kits (R5, D3) and Illumina Nextera kits (R7). More details included in Tables 1 and 2. All libraries were then sequencing on Illumina HiSeq systems.

Analysis of sequencing data. Sequences were aligned using BWA, GATK, Novoalign, Isaac, or LifeScope software. The variants were called using GATK, SAMtools, Annovar, CarpeNovo, Isaac, LifeScope and in-house pipelines. More details can be found in Tables S1 and S2. After identification of candidate variants in *ACTL6B*, their segregation was confirmed by Sanger sequencing using standard protocols.

Fibroblast reprogramming to induced pluripotent stem cells (iPSCs) Fibroblasts were obtained from biopsies or from Coriell (Table S3), and cultured in DMEM (Invitrogen) supplemented with 10% bovine serum albumin (Invitrogen). Fibroblasts were reprogrammed using episomal reprogramming vectors containing Oct4, Sox2, Myc3/4, Klf4, ShRNA P53 (ALSTEM) and a puromycin resistance gene using a Neon Transfection System (Invitrogen). Following transfection, cells were plated on tissue culture plates coated with Matrigel (Corning) in TesR-E7 media (Stem Cell Technologies) supplemented with 2ug/ml puromycin (Sigma). Following 48hrs of puromycin selection, fresh TesR-E7 media was exchanged, until distinct and robust iPSC colonies formed, at which point mTESR1 media (Stem Cell Technologies) was used to maintain and proliferate the colonies. Quality control experiments for iPSCs include mycoplasma testing, short tandem repeat profiling to ensure no sample mix-ups, assessment of endogenous pluripotency factor, immunocytochemistry for pluripotency markers, and molecular karyotyping.

Molecular Karyotyping To ensure no chromosomal abnormalities occurred as a result of iPSC induction or gene editing, DNA from all generated iPSC lines was sent to Prince of Wales Hospital (Shatin, Hong Kong) for sequencing on an Ion Torrent Hi-Q Sequencer (Thermofisher). Samples were sequenced with an average of 4 million 150bp reads per sample, for an average coverage of 0.0014X. Analysis was preformed using CNV-Seq[12]. Positive controls included cells of origin and cells from families with first-degree relationships where we could detect Mendelian inheritance of CNVs >1Mb.

Differentiation of iPSCs to forebrain neural progenitor cells (NPCs) iPSCs were differentiated to forebrain NPCs according to our previously described methods [13; 14]. iPSC colonies were dissociated and resuspended in DMEM/F12 media supplemented with N2 (Invitrogen) B27 (Invitrogen),and BSA [1 mg/ml], Y27632 [10 μM] (AdooQ Bioscience), SB431542 [10 mM](Selleckchem), and Noggin [200 ng/ml](GenScript), onto non-adherent plates to form organoids. After one week of maintenance as organoids, cells were dissociated and plated on Matrigel coated plates in DMEM/F12 supplemented with B27, bFGF (20ng/ml), EGF (20ng/ml), and laminin[1ug/ml] for a further seven days of differentiation, with media exchanged every three days. Cells were assessed for NPC morphology, and stained for markers of forebrain NPCs (PAX6, SOX2, TUJ1) and OCT4.

Differentiation of NPCs to Post-mitotic Neurons For short term (5 days) differentiation, NPCs were plated in DMEM/F12 media supplemented solely with B27. If longer term (>5 days) differentiation was required, NPCs, were plated in BrainPhys SM1 (Stem Cell Technologies) and N2-A supplemented media (Stem Cell Technologies). 50% of this media was exchanged every three days. Previous work has shown that neurons generated using this methodology express both GABAergic (~30%) and Glutamatergic (60%) markers[14] and are negative for midbrain markers, such as tyrosine hydroxylase. Approximately 5-10% of cells stain for GFAP, an astrocyte marker.

Whole Cell Recordings For whole-cell patch-clamp recordings, individual coverslips containing differentiated hIPSC-Derived Neurons were transferred into a heated recording chamber and continuously perfused (1 ml/min) with BrainPhys™ Neuronal

Medium (Catalog # 05791; StemCell Technologies) bubbled with a mixture of CO_2 (5%) and O_2 (95%) and maintained at 25 °C. Whole-cell patch clamp recordings were obtained using borosilicate pipettes (3–6 MΩ), filled with intracellular solution that contained the following (in mM): 5 HEPES, 2 KCl, 136 potassium gluconate, 5 EGTA, 5 Mg-ATP, 8 creatine phosphate, and 0.35 GTP. The pH was adjusted to 7.27 with KOH, and the osmolarity adjusted with distilled water or concentrated potassium gluconate if needed to between 295 and 298 mOsm with an osmometer (3320; Advanced Instruments). After a recording was completed, the nominal membrane potential in voltage- and current-clamp recordings was corrected for the calculated 10 mV liquid junction potential. All potential values reported reflect this correction. Once whole-cell recording had been established, neurons were routinely held in voltage clamp at -70 mV except when examining changes in the resting membrane potential and rheobase, which was performed in current clamp. Cells were only studied if they exhibited a stable holding current and access resistance for at least 10 min before experimental manipulations. Data were acquired using a Digidata 1550A/ Multiclamp 700B (Axon Instruments) and Clampex 10.5 (Molecular devices). Currents were filtered at 2 kHz and digitized at 20 kHz.

CRISPR/Cas9 gene editing A double nickase CRISPR/Cas9 gene editing system with a Paprika RFP (pRFP) reporter and gRNA targeting the first exon of the *ACTL6B* was used for KO experiments. For ACTL6Bext33 repair experiments, a wild-type CRISPR/CAS9-pRFP gene editing system was used to target the mutation in the stop codon of exon 14 of *ACTL6B*. One µg of construct was added per transfection reaction, and transfection was carried out simultaneously with iPSC induction to ensure clonality, as previously described[14]. Following transfection, cells were selected for puromycin

resistance and RFP visualization as described[8] allowing for cell expansion from a single edited fibroblast. Potentially edited colonies were expanded and stored as cell lines after which DNA was extracted and Sanger sequenced at Genome Quebec.

RNA Sequencing RNA samples with RIN values >9.0 were submitted to Genome Quebec for RNA sequencing. Eight libraries were run per lane of an Illumina HiSeqV4 2500 flow cell (125 bp paired-end reads), which achieved an average of ~40 million reads per library. For bioinformatic processing, we used FASTX-Toolkit, TopHat[15] Bowtie2[16], and Cufflinks2[17] with default parameters to preprocess, align, and assemble reads into transcripts, estimate abundance, and test differential expression. More detailed methods can be found here[18].

Western Blot Cells were lysed with RIPA buffer (Sigma) supplemented with SIGMAFAST™ Protease Inhibitor Tablets (Millipore-Sigma). Protein concentrations were determined using a Pierce BCA Protein Assay Kit (ThermoFisher). Approximately 15 µg of protein was loaded per well in Mini-PROTEAN® TGX Stain-Free™ Precast Gels (Biorad). Gels were run at 150V for approximately 75 minutes, and then transferred to a nitrocellulose membrane using a Trans-Blot® Turbo™ Transfer System (Biorad). Membranes were blocked in 4% non-fat milk dissolved in TBS-T buffer (tris-buffered saline-tritonX; Sigma-Aldrich) for twenty minutes, and then incubated with primary antibodies overnight at 4^0C with shaking. Blots were washed three times in TBS-T for five minutes, and then incubated with appropriate mouse or rabbit secondary antibodies for one hour at room temperature. Blots were washed a further three times in TBST for five minutes, then imaged using a ChemiDoc™ XRS+ System (Biorad). Blots were imaged and analysed using ImageLab (Biorad) software, and statistical analysis was

preformed using student T-tests when two samples conditions were present and a one-way ANOVA when more than two sample conditions were present. Blots were normalized to β-actin. Further details on the antibodies used for WB can be found in Table S5.

Quantitative PCR Reverse transcriptions were done on the total RNA fraction in order to obtain cDNA in 40 µl volume containing 1 µg of total RNA, 0,5 µg random primers, 0.5 mM dNTPs, 0,01 M DTT and 400 U M-MLV RT (Invitrogen). The reactions were performed in a total volume of 20µl volume on a 384 well plate either using an Applied Biosystems 7900 HT (Applied Biosystems) or a QuantStudio 6 (Thermofisher) PCR Machines. For each well, PCR mix included 10µl of Power SybrGreen PCR Mastermix (Life Technologies), 1 µl of primers/probe mix, 2 µl of cDNA, H20 up to 20 µl. Serial dilutions of a mix of cDNA ranging between 0.003052 ng and 50 ng were used to generate a calibration curve for an absolute quantification. Protein levels were given as a ratio between the relative quantities of the gene of interest and the endogenous control. GAPDH was used as internal control for normalization. The normalized expression levels were then compared between cell lines using either a student's t-test or an ANOVA with post-hoc t-test. Further details on the primers used for qPCR can be found in Table S6.

Immunofluorescence Adherent Cells were washed with PBS, then fixed with 3% paraformaldehyde (Sigma-Aldrich) on slides for fifteen minutes. Samples were permeabilized with 0.5% TX-100 (Sigma-Aldrich) in 0.5% PBS-BSA for fifteen minutes, and then blocked in 0.5% PBS-BSA for an additional fifteen minutes. Primary antibodies were added in appropriate dilutions (Table S5) in 0.5% PBS-BSA and added to samples

for 30 minutes. Samples were washed in 0.5% PBS-BSA containing an appropriate dilution of secondary antibody (Table S5) was added to the samples and incubated for thirty minutes in the dark. Samples were washed with 0.5% PBS-BSA. Samples were then visualized on an Apotome Florescent microscope (Zeiss). Neurolucida Tracing Software (MBF Bioscience) was used to measure nuclei surface area, soma surface area, and projection length. Images were processed and scale bars added in Image J.

Chromatin immunoprecipitation (ChIP) sequencing Samples were prepared for CHiP-Seq and CHiP-qPCR using a Magna ChIP-Seq™ kit (Millipore-Sigma). Cells were cross linked at day 0 and day 5 of differentiation by immersion in 37% formaldehyde. Glycine was added at a final concentration of 125uM to the samples to inactive cross-linking. DNA was sheared using a S220 Sonicator (Covaris), and precleared using a protein A or G agarose beads. All samples were then probed using both a mouse monoclonal (Santa Cruz, sc-17796) and rabbit polyclonal (Santa Cruz, sc-10768) antibody directed against BRG1 overnight at 4^0C. A IGG control was ran for both rabbit polyclonal and mouse monoclonal antibodies using a pooled sample composed of equal parts of all samples used for CHiP. A 0.2M glycine solution pH 2.6 was used for elution of cross-linked proteins and DNA from the beads. DNA was purified using Agencourt® AMPure® XP Beads (Beckman Coulter). Libraries were constructed using an NGS Library Preparation Kit (Millipore-Sigma) and sent to Genome Quebec, where they were sequenced using a Illumina HiSeqV4 2500 flow cell (125 bp paired-end reads) with between 11-12 samples sequenced per lane.

ChIPSeq Analysis

Quality trimming and pre-processing Sequencing adaptors were clipped using Trim

317 Galore. Quality trimming was done with same tool. A phred score cut-off value of 20 was
318 used. Reads shorter than 20bp were filtered out. Reads were aligned to the Human
319 Reference Genome (hg19) using BWA software version 0.7.10. Resulting bam files
320 were filtered for minimal mapping quality (MAPQ ≥ 20) and all alignments with samflag 4
321 (read unmapped) were excluded using SAMtools (version 0.1.19). Duplicates reads were
322 removed using the MarkDuplicates module of Picard (version 1.141) with the option
323 REMOVE_DUPLICATES=true.
324
325 ***Peak calling*** The identification of ChIP-seq enriched regions (peaks) was performed
326 using MACS2 (version 2.1.1); (macs2 callpeak --format BAM --broad --nomodel -q 0.05
327 --broad-cutoff 0.1 --extsize 500). Differential binding-sites analysis were done using the
328 DiffBind Bioconductor R package (version 2.6.6)[4]. Diffbind calls some of the DESeq2
329 (version 1.18.1) functions to perform the contrast analysis between pairwise
330 p.*427Aspext*33 or Control D5 vs D0 groups (dba.analyze (method = DBA_DESEQ2)).
331 For each comparison, DiffBind generated a set of consensus peaks with the requirement
332 that peaks must be in at least two of the samples (minOverlap = 2). Standardized
333 differential analysis was then performed using the following default settings for
334 dba.analyze: method=DBA_DESEQ2, FDR <= 0.05, bSubControl parameter set to
335 TRUE, bFullLibrarySize set to TRUE. Thus, raw number of reads in the control sample
336 was subtracted and the library size was computed for each sample and used for the
337 normalization. sizeFactors is called with the number of reads in the BAM files for each
338 ChIP sample, divided by the minimum of these. The final normalized counts returned are
339 the raw reads (adjusted for control reads) divided by the normalization factors (result of
340 calling sizeFactors()). Significantly different peaks were then annotated with HOMER
341 (version 4.7)[6] using RefSeq annotations (distal_distance = -10000, distance5d_lower
342 =-10000, distance5d_upper = -100000, gene_desert_size=100000, proximal_distance=-

343 2000).

344

345

Results

Identification of French Canadian families with homozygous mutations in *ACTL6B*

By exome sequencing of families with neurodevelopmental disorders in Quebec, we identified a family with two children with a homozygous mutation in *ACTL6B* that eliminates the stop codon (c.1279del, NM_016188.4) and extends the reading frame by an additional 33 amino acids (p.*427Aspext*33; NP_057272.1; Individual R3, Figure 1, Table 1, Table S1).

Sequencing both affected children, their unaffected older brother, and both parents from family R3 revealed that c.1279del was the only mutation identified in the family that was protein altering, followed an autosomal recessive inheritance model and was absent from all genomic databases. Both parents and the unaffected brother were carriers, and all are healthy. The phenotype of the disorder is severe: both brothers died early (4 and 6 years) of aspiration asphyxiation, were non-verbal, non-ambulatory, and required 24-hour care for all needs. Parents reported incessant crying (10+ hours per day), seizures beginning at 3 months, and sleep difficulties, (Table 1). An MRI of the brain was provided and had no indications from the reviewing radiologist. Careful tracing of the lineage of family R3 using Catholic Church records[7] revealed a common ancestor, which we determined to be the most likely origin of the mutation in Family R3 (Figure S1A and Supplemental Methods). We genotyped five other members from family R3 across four generations and could identify appropriate inheritance of the mutation from the predicted founder (Figure S1B). The R3 parents of the proband can be traced to a brother and sister going back six generations in the mother and five generations in the father, an event unknown to the R3 parents prior to birth of the probands (Figure S1B).

Another French Canadian family (defined as both great grandparents being born in the province of Quebec, Canada) with child R10 (Table 1) also had this same mutation with almost identical phenotype, suggesting that this mutation is not private to the R3 family but rather may be a specific but rare variant in the French Canadian population. We assume that these families are distantly related but could not identify the branch point at which the pedigrees may overlap between families R3 and R10.

Biallelic mutations in *ACTL6B* cause a severe neurodevelopmental disorder

We were able to identify eight additional families with a similar phenotype (Table 1, Table S1) with biallelic mutations. A majority of these identified mutations resulted in premature termination codons, and were located in highly conserved sequences (Figure 1B-C). We considered it very likely that most of these mutation sites resulted in nonsense mediated decay (NMD) of the transcript, as they occur well in advance of the penultimate exon[19], and strongly suggests that the disease is due to loss of function of the *ACTL6B* gene. However, some mutations, including the c.1279del mutation were located in the final exon of *ACTL6B* (Figure 1B), and were therefore not predicted to lead to NMD[19]. Heterozygous stop mutations are present in healthy parents, suggesting a recessive disorder. Selected case vignettes can be found in the Supplemental section.

De novo missense mutations at specific loci in *ATCL6B* cause a different, severe neurodevelopmental disorder

Over the course of identifying subjects with mutations in *ACTL6B*, we found ten individuals with heterozygous *de novo* missense mutations in *ACTL6B* with hypotonia, intellectual disability, developmental delay, autism, and Rett-like stereotypies such as handwringing (Figure 1, Table 2, Table S2). Detailed case vignettes of some subjects

are presented in the Supplemental section. This was surprising, given that we observed heterozygous stop/Frameshift mutations in healthy individuals arguing for a recessive inheritance model. Nine of ten of these individuals possess the same well conserved c.1027G>A mutation (Figure 1C and Table 2). p.Gly343Arg (NM_016188.4, HG19:chr7:100244258; Exon 12), is not seen in the 60,706 ExAC subjects. The same holds true for the other observed variant, p.Asp77Gly (NM_016188.4; HG19: chr7: 100253082; exon 3), both of which are likely gain-of-function mutations since heterozygous stop mutation carriers have no disease. 3D modeling of the *de novo* dominant and the recessive biallelic mutations (Figure 1D) shows no spatial clustering of mutation sites.BAF53B has an actin-related domain, which is subdivided into four subdomains[20]. Subdomain I and III are structural, and also contain residues that interact with ATP[21]. Subdomain II is the smallest domain, and enables the protein to have polar and non-polar orientations. Previous work has shown that mutations in this subdomain impair dendritic outgrowth[4]. Subdomain IV interacts with subdomain 1[20] and is necessary for the interaction of the protein with actin[21]. We mapped these subdomains onto a model of BAF53B derived from the S.cervisiae; ARP4 structure, and found that the variants occurred in all subdomains. Specifically, p.Phe147del, p.Cys425, p.Arg130Gln and p.Gln411* variants occur in Subdomain I, the p.Asp77Gly variant occurred in Subdomain II, p.Gly343Arg, p.Gly349Ser and p.Arg130Gln occur in Subdomain III, and p. Gly425*, occur in Subdomain IV (Table 1-2). We did not find any concentration of mutations in a particular domain.

Two other BAFopathies, Nicolaides-Baraitser syndrome (MIM:600014) and Coffin-Siris syndrome (MIM: 614556), so called because they affect genes that code for proteins that can be incorporated into the BAF complex, have sparse scalp hair and

422 coarse facial features, though this is a wide spectrum in affected individuals. We
423 obtained images of several probands in this study and did not observe coarse features in
424 the majority of subjects (Figure 1A). However, in individuals with the dominant mutations,
425 we did find common features such as a wide mouth, diastema and bulbous tip of the
426 nose. In the case of MRI brain structure this was grossly normal, with subtle but not
427 specific features (common across many MRI scans of children with neurodevelopmental
428 diseases) detected for some individuals (Table S1, S2)).
429
430 **Modeling the p.*427Aspext*33 variant in human neurons**
431 Human stem cells are a powerful model for functional genetic studies as mutations can
432 be assayed on a relevant genetic background and are amenable to genetic engineering.
433 All iPSC lines generated in this study had normal chromosomal integrity, presented
434 typical hallmarks of pluripotency (Figure 2A), including expression of endogenous
435 pluripotency genes (Figure S2A-B), and had the capacity to differentiate into all three
436 germ layers (Figure S2C). iPSCs were utilized to generate forebrain neural progenitor
437 cells (NPCs), which expressed neural and forebrain specific markers (Figure 2B; Figure
438 S3). Mature neurons generated from wild type cells expressed markers of cortical
439 neurons and displayed electrophysiological characteristics typical of high quality iPSC-
440 derived neurons, including spontaneous action potentials and excitatory post-synaptic
441 currents (Figure 2D-F).
442
443 To assess the validity of iPSC-derived neurons to model *ACTL6B* mutation
444 syndrome, we sought to recapitulate the developmental expression increase[2] in *ACTL6B*
445 in wildtype neurons, where *ACTL6B* expression is absent from dividing cells but is
446 present in post-mitotic cells[2]. We found that *ACTL6B* increased in expression from day 1

to day 5. To minimize time in culture which can increase experimental variation, we selected five days differentiation as our timepoint for post-mitotic transcriptomic analysis, where we could be confident *ACTL6B* would be well expressed (Figure 3A and 3B). To characterize the basic expression pattern of key genes involved in the BAF complex in both p.*427Aspext*33 and control cells, we assessed the expression of *ACTL6B*, *ACTL6A* and *SMARCA4* (MIM: 603254) a core DNA binding component of the BAF complex. Genes were assessed at Day 0 (D0) and Day 5 (D5) of differentiation. *ACTL6B* expression increased significantly in both p.*427Aspext*33 and control cells as cells differentiated. We also detected a significant decrease of *ACTL6B* in p.*427Aspext*33 compared to control cells at D5 (Figure 3C). *ACTL6A* had high expression in proliferating cells with a significant decrease after 5 days, but yet was still clearly expressed at day 5 in both control and p.*427Aspext*33 cells (Figure 3C). We detected no significant difference in the expression level of *SMARCA4* between any cell line or timepoint (Figure 3C). To confirm and validate these mRNA based data, we performed western blot on protein extracted from p.*427Aspext*33 and control cells at proliferative and post-mitotic timepoints (Figure 3D). These data suggest that there is no difference in protein level of any of BAF53A, BAF53B, and BRG1 between control and p.*427Aspext*33 cells. By developmental period (proliferating and post-mitotic) we observe consistent protein levels of BAF53A and BRG1, and absent BAF53B in proliferating cells.

Engineered homozygous deletion of *ACTL6B* in human neurons causes severe loss of dendrites

What is the function of *ACTL6B* in developing human cells and what is its role in human disease? Our previous experiments suggest that BAF53B is specific to post-mitotic cells, as reported in rodents[22], so we opted to inactivate *ACTL6B* to determine cellular phenotypes resulting from complete gene loss.

We knocked out *ACTL6B* from control human cells using a clonal genetic engineering technique[23] (Supplemental Methods). We generated two independent *ACTL6B* knockout cell lines that had different homozygous frameshift mutations in exon 1 (KO1 and KO2; referred to collectively as KO), and compared them to the isogenic cell line that had undergone no editing event (Control) (Figure 4A-B). The use of two independently edited cell lines with the same outcome (homozygous loss of *ACTL6B*) is one way to ensure against cell line artefacts, where we do not expect the same artefact to be present in both cell lines. To further ensure this, we Sanger Sequenced the five genomic regions most likely to be edited by the gRNAs used, all of which were unedited, suggesting no off-target effects, as has been reported and systematically assessed previously[24]. We also performed long-range (1.6Kb) sequencing to ensure that these mutations were in fact homozygous and not due to a large deletion in one allele, in addition to DNA based qPCR to confirm equal gene dosage between edited and unedited lines (Supplemental Methods). Following clonal gene editing and careful genomic integrity assessment, we planned to investigate dendritic length anomalies in a more mature neuronal state, since mouse KO *Actl6b* neurons show deficits in dendrite development[4]. To do this, we differentiated human *ACTL6B* KO cell lines and their matched isogenic controls for 15 days (D15 – a timepoint where we routinely see extensive neuronal arborisation in culture[23]) and confirmed the loss of *ACTL6B* expression at the mRNA and protein level (Figure 4C-D). We used MAP2 and TUJ1 as dendritic and neuronal markers, respectively, since these are routinely used in

neuroscience research for this purpose [25; 26]. We observed virtually no MAP2 staining in *ACTL6B* KO cells, while MAP2 was clearly present in most cells in the isogenic controls (Figure 4E). We also observed a larger nuclear size in the deleted cells, as assayed by DAPI, an effect that is obvious on cell examination (Figure 4F).

The p.*427Aspext*33 mutation phenocopies *ACTL6B* KO dendritic deficits and is reversible upon biallelic genetic repair

From our genotype-phenotype data from affected individuals and their first degree realtives, we reasoned that recessive mutations cause a loss-of-function of *ACTL6B*, and thus may mimic the cellular phenotype of the engineered *ACTL6B* KO cells. To demonstrate this, we reasoned that using these cell lines and comparing them to a clonally repaired version should provide interpretable data.

We biallelicaly repaired the ACTL6Bext33 line to a wildtype genotype and simultaneously reprogrammed these edited cell lines, where we had several unsuccessful repairs that could be used as isogenic controls. Homology directed repair was performed using a wildtype template in p.*427Aspext*33 fibroblasts plated at low density and iPSCs colonies derived from a single fibroblast were isolated, ensuring clonality and purity of repair[23]. After iPSC expansion of many colonies, we extracted DNA and Sanger sequenced around the mutation site (Method S2-S4). A colony with c.1279del mutation repaired to a wildtype genotype was identified and labelled as Successful Repair (SR) and differentiated to NPCs in tandem with an Unsuccessful Repair (UR) line, which was derived from a colony that received the CRISPR complex and repair template but where no editing event occurred (Figure 5 A-B). We differentiated these cells from NPCs to D15 neurons and then stained for MAP2 and TUJ1, identical in design to the KO study. As shown in Figure 5D-E, affected individual

519 cells recapitulate the loss of MAP2 and increased nuclei size observed in the KO, a
520 result that is reversed on repair of the homozygous base change in *ACTL6B*. The
521 similar cellular phenotype between affected individual and engineered KO neurons
522 suggest that the ACTL6Bext33 recessive mutation causes similar deficits to the
523 complete KO, and thus could be interpreted as causing a loss-of -function.

524

525 **Loss of dendrites due to loss of function of *ACTL6B* is likely due to delayed**
526 **maturation of young neurons**

527 Is the observed decrease in MAP2 staining due to immature differentiation,
528 differential differentiation, or a specific deficit in dendrite development? To try to address
529 these questions, we first asked whether the cell types in each condition were equivalent.
530 To investigate this question we stained D15 cultures from repaired and KO cells and
531 their control with an astrocyte (GFAP) and a neuronal marker (TUJ1), with the
532 hypothesis that perhaps deficits in *ACTL6B* bias NPCs towards becoming astrocytes.
533 Figure S4A shows the results of this experiment; we could not detect different numbers
534 of cells that stained for GFAP. We include in this experiment a positive control where we
535 add 0.1% BSA which can glialize cell cultures. To support the idea that deficits of
536 *ACTL6B* do not lead cell cultures to become more glial and to provide more specificity
537 than just GFAP, we assessed the transcriptomic data of p.*427Aspext*33 and control
538 cells we had generated in an RNA-Seq experiment. We found no consistent pattern in
539 mRNA expression levels of glial markers *ALDH1L1, GFAP*, and *GJA1* and neuronal
540 markers *RBFOX3* and *TUBB3* to suggest an increase in expression of glial related
541 genes in ACTL6Bext33 cells compared to control cells (Figure S4B). These data
542 indicate that deficits in *ACTL6B* do not lead NPCs to become more astrocytic. We

543 therefore ruled out the loss of MAP2 staining being due to cells being pushed towards an
544 astrocytic fate.

545 As a simple measurement of differentiation, we opted to photograph control,
546 ACTL6Bext.33, ACTL6B KO and Repair cells across several developmental timepoints.
547 Figure S5 shows that in contrast to repaired and control cell lines, unrepaired and KO
548 *ACTL6B* cells are not branched prior to day 20, whereas at day 25 through day 50, all
549 lines show branching.

550 These data suggest that deficits in *ACTL6B* lead to a delay in differentiation in
551 early post-mitotic states. This delay in differentiation, if true *in vivo*, may lead to cell
552 connectivity deficits.

553

554 **The p.*427Aspext*33 mutation alters BRG1 genomic binding and affects gene**
555 **expression**

556 This project began with the index case R3 (p.*427Aspext*33) which had fibroblasts
557 collected prior to mutation identification, thus our study is heavily biased towards this
558 case. To this end, we opted to continue experiments with these cells, with the idea that
559 we might recruit cells from other subjects or design exogenous templates for validation
560 studies.

561

562 We wanted to understand the molecular consequences of the p.*427Aspext*33
563 variant and how this might lead to neurodevelopmental deficits. Due to a lack of ChIP
564 grade antibodies directed specifically to BAF53B, we chose to perform a ChIP-Seq
565 experiment targeting BRG1, a key subunit of the BAF complex with ATPase activity that

566 is found both BAF53B and BAF53A containing BAF complexes [11]. We chose the D0 and
567 D5 time points for proliferating and post-mitotic cells respectively, and performed ChIP in
568 control and ACTL6Bext33 cells using eight replicates per subject per time period (32
569 ChIP experiments). We performed several QC experiments with different anti-BRG1
570 antibodies prior to sequencing to ensure appropriate parameters (not shown), and chose
571 two antibodies to provide overlapping datasets of Brg1-containing BAF complex binding
572 (Figure 6A). After sequencing and QC, we analyzed differential binding in D5 cells to
573 understand how the genomic targeting of Brg1-containing BAF complexes may be
574 altered by a mutant BAF53B subunit. ChIP peaks were called in at least 2/8 lines, and
575 differential analysis used reads from all replicates within the peak. 10,222 peaks were
576 common across all data points (Figure 6B), suggesting that BRG1 remains mostly at the
577 same location in the genome, even in mutant *ACTL6B* cells and irrespective of
578 developmental state.

579 We focused our primary analysis on D5, since this is when *ACTL6B* is
580 expressed, and tried to determine whether there was differential binding of BRG1 at
581 peaks called in both p.*427Aspext*33 and control cells. Using FDR <0.05, we found no
582 significant differences; however, using an uncorrected p-value of 0.05 revealed 382
583 common genomic regions that were significantly differentially bound and every one of
584 these showed increased binding in affected individual cells (Figure 6C). Loss-of-function
585 of BAF53B may lead to increased affinity or stabilization of the BAF complex to its
586 genomic targets, possibly through retention of BAF53A. More than half of the 382 sites
587 that BRG1-containing BAF complexes were found to bind to were associated with genes
588 (Figure 6C). PANTHER GO terms associated with the differentially bound regions were
589 related to cell adhesion and neurodevelopment (Figure 6D). This list included autism
590 associated genes including *AUTS2, PTEN, FOXP2*, and *SMARCA2*.

To further assess whether mutant *ACTL6B* leads to increased binding of BAF to genomic regions, we performed a within-subjects analysis in proliferating (D0) and differentiating (D5) cells, looking for peaks present at both developmental stages using FDR<0.05 for peak calling. While we did not find the same peaks that were called between cases and controls (suggesting the experiment was underpowered since we used 8 replicates in each block), we found evidence for a general decrease in BRG1 binding in differentiated cells compared to proliferating cells in those genomic regions present at both D0 and D5 in control conditions, in contrast to the p.*427Aspext*33 cells where there was a consistent increase in BAF binding at D5 compared to D0 (Figure 6E) at all sites. These data support the notion that a recessive *ACTL6B* mutation leads to increased association of BRG1 to certain areas of the genome.

How does genomic BAF binding affect gene expression and how might this differ when *ACTL6B* is mutated? We performed RNAseq in affected individual and control cells (n=4 independent replicates per subject) at D0 and D5 and looked only at those genes that were detected in the ChIPSeq analysis. We were interested in those genes that showed significant changes between D0 and D5 in the ChIPSeq data and which also showed significant change in the RNAseq data between D0 and D5 (within-subjects); Also, we selected those genes that showed RNAseq differences between mutant cells and control cells at D5 (Table S2). We highlight *TPPP* (Table S4), a microtubule binding protein involved in cell process extensions[27; 28], and *FSCN1*, which has been shown be involved in neurite shape and trajectory in prior studies in mice[29]. Due to their biological function and significance levels in our experiments, we chose to use *TPPP* and *FCSN1* expression levels to assess the external validity of our findings. We note the prevalence (Table S4) of genes that might be implicated in sphingolipid biology or myelin processing

(*SOX8*[30], *CERK*[31], and *A4GALT*[32]), consistent with Wu et al, (2007) who observed a severe myelination defect in *Actl6b* KO mice.

We used *TPPP* and *FSCN1* expression as output markers to assess direct versus correlational effects of mutant *ACTL6B*. We posed two initial questions to test direct versus correlational effects. First; does the *ACTL6B* KO show a similar pattern of expression to ACTL6Bext33 compared to its isogenic control? Second; do we see the opposite effect in the UR cells compared to the SR cells? We began by validating the RNA-Seq data, using the same RNA that was used to make RNA-Seq libraries (Figure 7A). Next, we examined the expression of these genes between D0 and D5 timepoints in *ACTL6B* KO cells and their isogenic controls, as well as in UR and SR cells. SR cells, when compared to UR cells showed a significant increase in *TPPP* and decreased expression of *FSCN1* as NPCs mature from D0 to D5. In *ACTL6B* knock-out cells compared to their isogenic controls, we observed significant and opposite effects to that observed with repaired cells: *FSCN1* expression did not decrease, while *TPPP* expression did not increase as the cells differentiated (Figure 7A). These data provide isogenic evidence that complete loss of *ACTL6B* and a repair of p.*427Aspext*33 recapitulate and reverse, respectfully, expression alterations in *TPPP* and *FSCN1* and suggest that expression changes in these genes are directly caused by disruption of *ACTL6B*.

External validity of *TPPP* and *FSCN1* expression levels as markers of an *ACTL6B* recessive, loss-of-function disease in human neurons using constructs derived from different *ACTL6B* variants.

External validity can be provided by KO rescue and by recapitulating expression effects using different mutations in *ACTL6B* identified in our cohorts (Figure 7B-D). If *TPPP* and *FSCN1* expression levels are markers of loss-of-function of *ACTL6B*, the exogenous re-introduction of *ACTL6B* on a KO background should help restore their expression towards levels observed in lines with wild-type *ACTL6B*. Further, expressing mutant *ACTL6B* to match other variants found in the recessive cohort should re-establish expression changes on an *ACTL6B* KO background. We therefore made *ACTL6B* constructs of two recessive mutations c.441_443 del and c.1275C>A, and the most prevalent dominant mutation c.1027 G>A, as well as the WT construct itself. Expressing these variants from trasnsiently delivered vector on an *ACTL6B* KO background, may give us an indication if the dominant and recessive variants mediate their effects through the same molecular pathways and cause similar effects on the expression of *FSCN1* and *TPPP*. At a D5 timepoint, cells transfected with WT *ACTL6B* showed decreased expression of *FSCN1* and increased expression of *TPPP*, consistent with what we observed in the initial KO experiment (Figure 7D), meaning that the WT construct can rescue the expression changes observed in *ACTL6B* KO cells. We observed that the two recessive variants (c.441_443 del and c.1275C>A) mimicked the effects observed in the recessive p.*427Aspext*33 variant, while the dominant mutation mimicked wildtype cells (Figure 7D).

Confirmation of dendritic deficits and gene expression markers using neurons derived from *ACTL6B* mutant c.617T>C/ c.724C>T

We obtained fibroblasts from individual R9 with compound heterozygous mutations in *ACTL6B* (c.617T>C, p.Leu206Pro and c.724C>T, p.Gln242*) (Table 1). We

663 induced the fibroblasts to become iPSCs, differentiated the iPSCs to D15 neurons and
664 confirmed the mutant genotype of this line (Figure 8A-B). We compared this "*ACTL6B*
665 compound heterozygous mutant" line to healthy control cells differentiated to a day 15
666 timepoint, and found a similar decrease of *MAP2* staining and increased nuclei size as
667 compared to the *ACTL6B* KO and ACTL6Bext33 lines (Figure 8C-D). Assessing the
668 expression of *TPPP* and *FSCN1* at D5 and D0 timepoints in the *ACTL6B* compound
669 mutant and control lines also produced results similar to those seen with the
670 ACTL6Bext33 line, with the *ACTL6B* compound mutant showing a lack of increased
671 expression of *TPPP*, as well as a lack of decreased expression of *FSCN1* during
672 differentiation compared to control cells (Figure 8E).

673

Discussion

These data describe two distinct neurodevelopmental diseases caused by dominant or recessive mutations in *ACTL6B*. This work positions *ACTL6B* mutations as causing both a recessive neurological disease characterized by severe epileptic encephalopathy, and a dominant intellectual disability syndrome with severe speech and ambulation deficits.

Previous studies have identified mutations in genes that code for other subunits of the nBAF and npBAF complexes that are capable of causing disease through dysregulated BAF function, collectively called "Bafopathies"[33]. The two foremost diseases among the Bafopathies, Coffin-Siris (CSS) (MIM: 135900) and Nicolaides–Baraitser (NCBRS) (MIM: 601358) syndrome show interesting parallels and differences to the diseases described here[34; 35]. While NCBRS is a monogenic disease, caused exclusively by mutations in *SMARCA2* (MIM: 600014) that are autosomal dominant, and CSS is a genetically diverse disease, and can be caused by mutations in *ARID1B* (MIM: 614556) and a variety of other genes that play a role in the BAF complex, that vary in their inheritance pattern, common symptoms appear to exist in both these conditions and the diseases described here. Common symptoms reported across conditions include intellectual disability, developmental delay, hypotonia and some form of dysmorphic facial features [34]. Like individuals with recessive mutations in *ACTL6B*, individuals with NCBRS also show early-onset seizures[36], and seizures are also reported in individuals with CSS, although they are not necessarily early-onset [34; 37; 38]. Individuals with NCBRS also show short phalanges[36], as observed in some individuals with dominant mutations in *ACTL6B*. However, some of the specific developmental symptoms observed in these diseases, such as sparse scalp hair[39] or an absent fifth digit[36] do not appear in individuals with either recessive or dominant mutations in *ACTL6B*. This could suggest

699 that while a general disruption of the BAF complex in a variety of protein subunits
700 neurodevelopment will inevitably lead to intellectual disability and developmental delay,
701 the specific protein subunit that is affected will determine the presence and nature of
702 dysmorphisms and epilepsy.

703 To understand why mutations in *ACTL6B* cause disease, we modeled the
704 disease in human NPCs and neurons. We first confirmed that *ACTL6B* expression was
705 induced upon neural cells becoming post-mitotic. We then went on to make several
706 different cell models in the hope of reducing variation across experimental variables. We
707 made forebrain progenitor cells from a healthy individual with experimentally induced
708 knock-out of *ACTL6B* to understand the effects of complete loss of the gene, in addition
709 to cells derived from individuals R9 and R3 with an isogenic engineered repaired cell
710 line.

711 While we cannot precisely determine the mechanism of the disease that appears
712 to be caused by bi-allelic mutations in *ACTL6B*, our results do illuminate several key
713 features of the etiology of the disease. First, the presence of BAF53B in the
714 ACTL6Bext33 cell line at D5 eliminates the possibility that the symptoms are caused by
715 an absence of BAF53B, as is likely the case in other variants of BAF53B where NMD is
716 predicted to occur[19]. Instead, it seems plausible that the symptoms are the result of a
717 loss of function of BAF53B stemming from changes in the structure of the protein. This
718 hypothesis is supported by our observations in the *ACTL6B* KO model, which shows
719 similar deficits in both MAP2 staining and the expression of key genes identified in the
720 ACTL6Bext33 that are regulated by BAF. *ACTL6B* KO cells expressing the recessive
721 mutations in *ACTL6B* observed in our recessive cohort fails to rescue aberrant
722 expression of genes, whereas reintroduction of wildtype *ACTL6B* does, strongly
723 suggesting that the phenotype is the result of a loss of function.

However, how the recessive mutations render BAF53B non-functional could be due to one of several possibilities. Perhaps the most intuitive answer is that mutations disrupt the ability of BAF53B to bind to the BAF complex. If this fails to occur, this might allow BAF53A to remain bound in the complex. Given that there are a great many BAF complexes that dynamically exchange parts to affect cell differentiation at any one time, a high proportion of BAF53A in BAF might cause increased affinity of BAF to the genome in a differentiating cell state compared to both a proliferating cell state when BAF53B is absent or a differentiated cell state where BAF53B is present but not functional and/or when the interaction with the complex is impaired. The increased presence of BAF53A in the BAF complex, associated with a more proliferative neuronal cell state, might also explain the delayed differentiation we observed in disease cells. Another explanation could be that recessive mutations do not prevent BAF53B from binding to the BAF complex, but instead prevent the various components of the complex from interacting properly, and thus prevent the BAF complex from interacting with the genome and other proteins in yet unknown ways. Finally, there is the possibility that recessive mutations do not disrupt BAF complex function significantly at all, but instead prevent BAF53B from properly interacting with the other complexes such as SRCAP[40], TIP60/NuA4[19] and INO80[41]. Future work will need to look at how mutant BAF interacts with different proteins.

With respect to the dominant mutation identified in eight unrelated individuals, we failed to observe the transcription effects we found in the KO, *ACTL6B* compound heterozygous mutant or the ACTL6Bext33 cells, suggesting dominant and recessive mutations in *ACTL6B* cause disease through distinct molecular pathways. This is also consistent with the observation of different symptoms in individuals with recessive/

749 dominant mutations in *ACTL6B*. Based on the limited molecular information we have for
750 dominant mutations, there exists many potential explanations for how a point mutation in
751 *ACTL6B* might cause the observed symptoms. Given that these subjects all have a
752 functioning copy of BAF53B which presumably incorporates normally into BAF or other
753 complexes, it is reasonable to suggest that the *ACTL6B* dominant mutations identified
754 here may be gain-of-function. One of the few clues that we have at this stage of
755 investigation is that the highly specific nature of the p.Gly343Arg variant suggests a very
756 precise interaction is being disrupted or created. Previous work in mice[42] has shown that
757 deletion of the hydrophobic domain of BAF53b results in a dominant negative form of
758 the protein, causing deficits in memory, LTP, and gene expression. These deficits were
759 likely caused by altering the ability BAF53B to interact with other proteins[42]. It is possible
760 that the dominant mutations observed in this study cause disease by altering the
761 hydrophobic domain of BAF53B through a similar mechanism.

762

763 Several genes of note may be important targets of the BAF complex at different
764 developmental stages. *FSCN1* is one of these and is strongly associated with the
765 formation of actin, particularly in early neurodevelopment[29; 43]. The lack of increase of
766 *FSCN1* observed in our models of *ACTL6B* dysfunction as cells differentiate may
767 therefore be the result of neuronal cells remaining in a more proliferative or immature
768 state due to an impairment in the ability of *ACTL6B* to transition the BAF complex from
769 promoting genes associated with proliferation to those associated with neuronal
770 outgrowth[44].

771 The stable expression levels of *TPPP* observed in models of *ACTL6B*
772 dysfunction as NPCs differentiate may reflect the cytoskeletal changes observed both
773 within our own models and in the deficits in dendritic spine and synapse function

774 observed in mouse models of *Actl6b* KO. It should also be noted that our ChIP-SEQ
775 data that initially highlighted these genes as being dysregulated is based upon only
776 BRG1-containing BAF complexes. As BRG1 and BRM are mutually exclusive
777 components of the BAF complex that are both found in dividing and post-mitotic neural
778 cells[11], it is possible that the dataset we generated is only a partial picture of the regions
779 of the genome where BAF may bind in these cells.

780 This work brings together extensive clinical samples and human stem cell
781 modeling to demonstrate that mutations in *ACTL6B* in human cause severe neurological
782 disorders. Substantially more work will need to be done to understand the precise
783 mechanisms of how recessive or dominant mutations in *ACTL6B* affect incorporation into
784 the BAF complex, and how this incorporation can alter differential genomic binding and
785 gene expression patterns.

786

Supplemental Data

Supplemental Data can be found with this article online and includes five supplementary figures, four supplementary tables and supplementary methods which provide additional clinical details of individuals and further details of the generation, characterization, and quality control of the cell lines generated in this study.

Declaration of Interests

Amber Begtrup, Ingrid Wentzensen, and Amy Crunk are employees of GeneDx. Carl Ernst is president of ManuStem.com and has commercial interests with Stem Cell Technologies. The other authors declare no conflict of interest.

Acknowledgments

We acknowledge funding by: Scott Bell: FRQS- doctoral; Malvin Jefri: Government of Indonesia PhD award; Karla MV: CONACYT (Mexico) and MITACS; Jacques Michaud and Elsa Rossignol: Genome Canada and Génome Québec; GT and CE: Canada Research Chairs program; Naomichi M: AMED, MEXT, JST, MHLW, Takeda Science Foundation; CIHR grant to CE and PC. We are grateful to Gerald Crabtree who provided a custom antibody to BAF53B. CE is grateful to Family R3 who collaborated with his lab from mutation detection to human neuron modeling.

Figure Legends

Figure 1. Location of mutations in *ACTL6B* found in individuals with potential recessive or dominant disease causing mutations

A) Photos of individuals with *ACTL6B* mutations**.** Note broad mouth of individuals D1, D2, D3 and D7, diastema in D1, D3, D7, bulbous tip of the nose in all D individuals, and hypertelorism with telecanthi in individual D8. Lower right: MRI images of individuals with recessive *ACTL6B* mutations. For individual R4, note white matter T2 hyperintensity (arrows). For individual R8, note enlarged lateral ventricles and asymmetric gyral pattern (left, arrows). On the right, note thin corpus callosum (arrows). B) Linear graph of mutations in *ACTL6B* (introns not drawn to scale). C) Conservation of the residues affected by amino acid substitutions. D) 3D model generated with SWISSMODEL based on S. cerevisiae Arp4 (yeast homolog of ACTL6B), visualized with Swiss-PdbViewer showing that recessive mutations are not focused in one region. Note however that the dominant mutations seem to lie at the periphery of the protein thus they might affect protein-protein interactions.

Figure 2. Generation of iPSC-derived neurons for BAF53 studies

A) Representative images of quality control staining done on iPSCs. B) Representative quality control staining on NPC cultures. C) Representative staining of control cells for TUJ1 and MAP2 at D15 of differentiation. D) Representative trace of miniature EPSCs from D25 neurons held at -40 mv. E) Representative recordings showing spontaneous activity of D25 neurons in current-clamp mode. F) Trace of a hyperpolarizing pulse showing a depolarizing sag followed by multiple rebound action potentials. The first action potential is shown at a higher temporal resolution. All scale bars represent 40 µm

Figure 3. Comparison of control and ACTL6Bext*33 before and after expression of *ACTL6B*

A) Diagram illustrating the production of control and ACTL6Bext*33 iPSC-derived NPCs from fibroblasts B) *ACTL6B* expression normalized to *GAPDH* expression plotted against number of days of differentiation of NPCs. N=4, error bars represent standard error around the mean. C) Expression of key genes in the SWI/SWF complex in 706 ACTL6Bext*33 and control NPCs in proliferating and post-mitotic states. Genes are normalized to GAPDH expression. ($n \geq 3$) Student's t-test, *$P<0.05$, **$P<0.01$. H) Western blots assessing the level of proteins encoded by the genes displayed in G.

Figure 4. Generation and characterization of *ACTL6B* KO neurons reveals a loss of dendrites.

A) Diagram of the experimental approach taken to generate *ACTL6B* KO NPCs. B) Sanger sequencing traces of two *ACTL6B* KO lines. C) *ACTL6B* expression in control and *ACTL6B* KO NPCs at a D0 and D5 timepoint ($n \geq 3$) D) Western Blots assessing the

protein levels of *BAF53A/B* in ACTL6B KO lines. E) Representative TUJ1 and MAP2 staining of control and *ACTL6B* KO D15 immature forebrain neurons. F) Quantification of the surface area of the nucleus in the cell lines shown in E, (n>50). Student's t-test, *P<0.05, **P<0.01.

Figure 5. Repair of the *ACTL6B* c.1279del mutation restores morphological and dendritic deficits.

A) Schematic detailing *ACTL6B* CRISPR repair. B) Sanger sequencing traces of a Successful Repair (SR) and Unrepaired (UR) cell line generated from ACTL6Bext*33 cell line. C) *ACTL6B* expression in SR and UR NPCs at a D5 timepoint (n=6) D) Representative TUJ1 and MAP2 staining taken from SR and UR forebrain immature neurons at D15. Scale bars represent 40µm. E) Quantification of the surface area of the nucleus and soma, and the length of projections in the cell lines shown in D, (n>50). Student's t-test *P<0.05, **P<0.01, ***P<0.001

Figure 6. ACTL6Bext*33 variant leads to increased binding of BRG1-BAF complex to the genome.

A) Diagram illustrating the ChiP-Seq experiment. B) Venn diagram showing overlap of genes that the BRG1 complex is bound to. C) Decreased binding at all 382 FDR significant sites in control cells compared to ACTL6Bext*33 cells (pink dots are significant, while blue dots are not). D) Proportion of BRG1 binding sites found in relation to their proximity to a gene. E) Gene ontology analysis of differentially bound regions. F) Within-subjects differential binding across developmental stages (D0 and D5) showing decreased binding in D0 compared to D5 in ACTL6Bext*33 cells (pink dots are significant, while blue dots are not). Genes showing a significant difference (FDR-adjusted p-values (Benjamini-Hochberg) ≤0.05) in D5 relative to D0 using a GLM as implemented in DESeq2.

Figure 7. External validity in multiple *ACTL6B* mutant models in human neurons

A) *TPPP* and *FSCN1* expression in initial RNA-Seq (n≥4) and qPCR (n≥3) data (ACTL6Bext*33 vs control); unrepaired (UR) ACTL6Bext*33 vs ACTL6Bext*33 Successful Repair (SR) (n=6); and *ACTL6B* KO vs isogenic control cells (n=5). Results are represented as mean ± SEM. Student's t-test *P<0.05, **P<0.01, ***P<0.001 B) Experimental plan for generation of multiple human neuronal cell lines expressing various mutant *ACTL6B* constructs. C) Brightfield and GFP images demonstrating high transfection of *ACTL6B* constructs. D) mRNA expression in transfected *ACTL6B* KO NPCs at D5 timepoints of *ACLT6B*, *TPPP,* and *FSCN1* (E) (n=3). Results are represented as mean ± SEM. Student's t-test *P<0.05, **P<0.01, ***P<0.001

Figure 8. Neurons derived from an individual with a compound mutation in *ACTL6B* show a similar phenotype to ACTL6Bext33 and ACTL6B KO neurons.

A) Schematic showing generation of ACTL6Bcompoundmutant NPCs B) Sanger sequencing traces of ACTL6Bcompoundmutant and control cell line at both identified point mutations in the *ACTL6B* gene C) Representative TUJ1 and MAP2 staining of control and ACTL6Bcompoundmutation immature forebrain neurons. D) Quantification of the surface area of the nucleus in the cell lines shown in E. E) *TPPP* and *FSCN1* expression in ACTL6Bcompoundmutant vs control cells at mitotic (D0) and post-mitotic (D5) timepoints (n>50). Student's t-test, *P<0.05, **P<0.01.

898 Table 1. Pathogenic variants and key clinical information of individuals with bi-allelic
899 mutations in *ACTL6B*.

Individual	R1	R2		R3	R4		R5		R6		R7	R8a	R8b	R9		R10
Inheritance	Recessive, homozygous	Recessive, Compound heterozygous. Similarly affected brother passed away at 5y		Recessive, homozygous. Similarly affected brother passed away at 4y	Recessive, Compound heterozygous		Recessive, Compound heterozygous		Recessive, Compound heterozygous		Recessive, homozygous.	Recessive, homozygous.	Recessive, homozygous. Sister of R8a.	Recessive, Compound heterozygous		Recessive, homozygous
Coding Change (NM_016188.4)	c.441_443delCTT	c.695delC	c.1275C>A	c.1279del	c.389G>A	c.556C>T	c.852C>G	c.740G>A	c.1231C>T	c.669+1G>A	c.289C>T	c.1045G>A	c.1045G>A	c.724C>T	c.617T>C	c.1279del
Protein Change (NP_057272.1)	p.Phe147del	p.Pro232Glnfs*24	p.Cys425*	p.*427Aspext*33	p.Arg130Gln	p.Gln186*	p.Tyr284*	p.Trp247*	p.Gln411*	splicing	p.Arg97*	p.Gly349Ser	p.Gly349Ser	p.Gln242*	p.Leu206Pro	p.*427Aspext*33
gnomAD MAF	0.0000014 44, no homozygotes	Absent	Absent	Absent	0.0000008132, no homozyg	Absent	Absent	Absent	Absent	Absent	0.0000004064, no homozyg	0.0000012119, no homo	0.0000012119, no homo	Absent	Absent	Absent

				ote s					ote s	zyg ote s	zyg ote s		
Age at assessment	3y F	5y M (passed away at age 5)	11m M (passed away age 5)	8y F		5m F		12m M (passed away age 2)	4y F	6y F	5y F	14m F	4.5y F
Head circum. In cm	43 (-3.5 SD)	NA	44 (3rd)	50.3 (10th %ile)		38,4 (-3.0 SD)		42 (-2.4 SD)	Nl	18 m 41. 5 (-3.8 SD)	4m 39 (7th %ile)	43 (-2,5 SD)	47 (-2.8 SD)
ID, DD	+, Severe	+	+	+, Severe		+, Severe		+, Severe	+, Severe	+, Severe	+, Severe	+, Severe	+
Speech	-	-	NA	-		NA		-	NA	-	-	-	-
Ambulation	-	-	NA	-		NA		-	NA	-	-	-	+, with support
Axial hypotonia	+	+	+	+		+		+	+	+	+	+	+
Limb spasticity	+	+	+	+		+		+	+	+	+	+	+
Feeding difficulties	+	+	+	-		+		+	+	+	+	+	-
Epilepsy	+	+	+	+		+		+	+	+	+	+	+
Seizures (age at beginning)	3 months	3y	NA	NA		2 months		Neonatal (25 days)	Infancy	Infancy	Infancy	Antenatal	9 months, infantile

											spasms
Seizure types	Myoclonias 2-6 per day	Complex partial	NA	NA	Tonic and myoclonic	Focal onset epilepsy, progressed to infantile spasms	NA	NA	NA	myoclonic seizures AND tonic seizures	Tonic and myoclonic
EEG anomalies	Multifocal epileptic activity	NA	Multifocal epileptic activity	NA	Multifocal epileptic activity	Multifocal interictal epileptiform spike discharges, lack of posterior dominant rhythm	Multifocal EEG abnormalities	generalized slowing of backgrounds rhythms	generalized slowing of backgrounds rhythms	Multifocal epileptic activity, esp. left hemisphere	Multifocal epileptic activity, esp. left hemisphere
MRI	Prominent subarachnoid spaces and small corpus callosum	Normal	Mild T2 hyperintensity in frontal periventricular white matter	Mild T2 hyperintensity in frontal periventricular white matter	2 months of age showed symmetric signal changes in the brainstem and in the dorsal medulla oblongata, possibly also around	3 w.o.: asymmetric ventricles, cortical dysplasia right parietal lobe. 9 m: cerebral atrophy, hypoplasia of corpus callosum	NA	MRI at 5mo: Significantly decreased white matter throughout, extr	10 mo: Periventricular leukomalacia with white matter volume loss,	Thin corpus callosum High signal intensity doral globus pallidus/putamen Some asymmetry gyral patern	At 3.5yo: Cerebral and cerebellar atrophy, thin corpus callosum

					the dentate nucleus			emely thin corpus callosum. Normal MR spectroscopy	overall brain volume loss, delayed myelination and thinning of corpus callosum. Normal MR spectroscopy		

900

901

902

903

904

905

906

907

908

909 Table 2. Pathogenic variants and key clinical information of individuals with *de novo*

910 mutations in *ACTL6B*.

Individual	D1	D2	D3	D4	D5	D6	D7	D8	D9	D10
Coding Change (NM_016188.4)	c.1027G>A	c.1027G>A	c.1027G>A	c.1027G>A	c.1027G>A	c.1027G>A	c.1027G>A	c.1027G>A	c.230A>G	c.1027G>C
Protein Change (NP_057272.1)	p.Gly343Arg	p.Gly343Arg	p.Gly343Arg	p.Gly343Arg	p.Gly343Arg	p.Gly343Arg	p.Gly343Arg	p.Gly343Arg	p.Asp77Gly	p.Gly343Arg
gnomAD MAF	Absent	Absent	Absent	Absent	Absent	Absent	Absent	Absent	Absent	Absent
Age at assessment	5y6m M	29y F	6y6m M	5y9m F	4y6m F	3y F	21y F	2y 6m F	8y F	12yF
Head circum. In cm	49 (-2.1 SD)	53 cm (11th %ile)	51 cm at age 5 yr (50th centile)	48.6 (-2.2 SD)	48 cm (2nd %ile)	48.0 cm (20th %ile)	52.2 cm (-2.0 SD)	45.5 cm (-0.1 SD)	50th-75th %ile	52 (-1,-2SD)
Degree of	Severe	Severe	Severe	Severe	Severe	Severe	Severe	Severe	Severe	Severe

ID/DD	re	re	re	re	re	re	e	e	re	re
Speech	-	-	-	10-20 words, Receptive skills better	-	-. Gestures.	-	-	-. Gestures. Receptive skills better	One word
Ambulation	-	+	limited	Delayed. Wide based gait	-	-	-	-	NA	Delayed. Wide based gait
Hypotonia	NA	+	+	NA	+	+	NA	-	NA	+
Autism spectrum disorder	NA	+	Unknown	+	NA	NA	NA	-	+	-
Features of ASD	NA	NA	+	NA	stereotypies	NA	hand wringing	-	NA	stereotypies
Seizure disorder	-	-	-	-	-	-	Infantile spasms and GTCS	-	NA	-
MRI	NA	NA	NA	NA	NA	thinning of the corpus callosum	Generalised atrophy at 2y	mild periventricular gliosis	NA	NI

Wide or prominent forehead	+	+	+	+	-	-	+	+	+	-
Hypertelorism	+	+	+	-	-	+	-	+	+	-
Wide mouth	+	+	+	-	-	-	+	+	NA	+
Short phalanges or nails	NA	+	-	+	-	-	+	-	+	-

911

912 **Web Resources**

913 BWA: http://bio-bwa.sourceforge.net/

914 GATK: https://software.broadinstitute.org/gatk/

915 MACS2: https://github.com/taoliu/MACS/wiki/Install-macs2

916 Trim Galore: http://www.bioinformatics.babraham.ac.uk/projects/trim_galore/

917 Bioconductor: http://bioconductor.org/packages/release/bioc/html/DiffBind.html

918 HOMER: http://homer.ucsd.edu/homer/

919 Neurolucida: https://www.mbfbioscience.com/neurolucida

920 Imagelab: http://www.bio-rad.com/en-ca/product/image-lab-software6\

921 Online Mendelian Inheritance in Man: http://www.omim.org

922 VarSome: https://varsome.com/

References

1. Meagher, R.B., Kandasamy, M.K., Deal, R.B., and McKinney, E.C. (2007). Actin-related proteins in chromatin-level control of the cell cycle and developmental transitions. Trends in cell biology 17, 325-332.
2. Biggar, S.R., and Crabtree, G.R. (1999). Continuous and widespread roles for the Swi-Snf complex in transcription. EMBO J 18, 2254-2264.
3. Lessard, J., Wu, J.I., Ranish, J.A., Wan, M., Winslow, M.M., Staahl, B.T., Wu, H., Aebersold, R., Graef, I.A., and Crabtree, G.R. (2007). An essential switch in subunit composition of a chromatin remodeling complex during neural development. Neuron 55, 201-215.
4. Wu, J.I., Lessard, J., Olave, I.A., Qiu, Z., Ghosh, A., Graef, I.A., and Crabtree, G.R. (2007). Regulation of dendritic development by neuron-specific chromatin remodeling complexes. Neuron 56, 94-108.
5. Peterson, C.L. (1996). Multiple SWItches to turn on chromatin? Curr Opin Genet Dev 6, 171-175.
6. Sudarsanam, P., and Winston, F. (2000). The Swi/Snf family nucleosome-remodeling complexes and transcriptional control. Trends Genet 16, 345-351.
7. Yoo, A.S., Staahl, B.T., Chen, L., and Crabtree, G.R. (2009). MicroRNA-mediated switching of chromatin-remodelling complexes in neural development. Nature 460, 642-646.
8. Staahl, B.T., and Crabtree, G.R. (2013). Creating a neural specific chromatin landscape by npBAF and nBAF complexes. Curr Opin Neurobiol 23, 903-913.
9. Vogel-Ciernia, A., Matheos, D.P., Barrett, R.M., Kramar, E.A., Azzawi, S., Chen, Y., Magnan, C.N., Zeller, M., Sylvain, A., Haettig, J., et al. (2013). The neuron-specific chromatin regulatory subunit BAF53b is necessary for synaptic plasticity and memory. Nature neuroscience 16, 552-561.
10. Santen, G.W.E., Kriek, M., and van Attikum, H. (2012). SWI/SNF complex in disorder: SWItching from malignancies to intellectual disability. Epigenetics 7, 1219-1224.
11. Sokpor, G., Xie, Y., Rosenbusch, J., and Tuoc, T. (2017). Chromatin Remodeling BAF (SWI/SNF) Complexes in Neural Development and Disorders. Frontiers in molecular neuroscience 10, 243-243.
12. Bakshi, R., Hassan, M.Q., Pratap, J., Lian, J.B., Montecino, M.A., van Wijnen, A.J., Stein, J.L., Imbalzano, A.N., and Stein, G.S. (2010). The human SWI/SNF complex associates with RUNX1 to control transcription of hematopoietic target genes. J Cell Physiol 225, 569-576.
13. Bell, S., Hettige, N., Silveira, H., Peng, H., Wu, H., Jefri, M., Antonyan, L., Zhang, Y., Zhang, X., and Ernst, C. (In Press). Differentiation of Human Induced Pluripotent Stem Cells (iPSCs) into an Effective Model of Forebrain Neural Progenitor Cells and Mature Neurons. Bio-protocol.
14. Bell, S., Peng, H., Crapper, L., Kolobova, I., Maussion, G., Vasuta, C., Yerko, V., Wong, T.P., and Ernst, C. (2017). A Rapid Pipeline to Model Rare Neurodevelopmental Disorders with Simultaneous CRISPR/Cas9 Gene Editing. Stem Cells Transl Med 6, 886-896.
15. Reynolds, B.A., and Weiss, S. (1996). Clonal and population analyses demonstrate that an EGF-responsive mammalian embryonic CNS precursor is a stem cell. Dev Biol 175, 1-13.

16. Langmead, B., Trapnell, C., Pop, M., and Salzberg, S.L. (2009). Ultrafast and memory-efficient alignment of short DNA sequences to the human genome. Genome Biol 10, R25.
17. Trapnell, C., Roberts, A., Goff, L., Pertea, G., Kim, D., Kelley, D.R., Pimentel, H., Salzberg, S.L., Rinn, J.L., and Pachter, L. (2012). Differential gene and transcript expression analysis of RNA-seq experiments with TopHat and Cufflinks. Nat Protoc 7, 562-578.
18. Chen, E.S., Gigek, C.O., Rosenfeld, J.A., Diallo, A.B., Maussion, G., Chen, G.G., Vaillancourt, K., Lopez, J.P., Crapper, L., Poujol, R., et al. (2014). Molecular convergence of neurodevelopmental disorders. Am J Hum Genet 95, 490-508.
19. Khajavi, M., Inoue, K., and Lupski, J.R. (2006). Nonsense-mediated mRNA decay modulates clinical outcome of genetic disease. European journal of human genetics : EJHG 14, 1074-1081.
20. Dominguez, R., and Holmes, K.C. (2011). Actin structure and function. Annual review of biophysics 40, 169-186.
21. Holmes, K.C., Popp, D., Gebhard, W., and Kabsch, W. (1990). Atomic model of the actin filament. Nature 347, 44-49.
22. Yoo, M., Choi, K.Y., Kim, J., Kim, M., Shim, J., Choi, J.H., Cho, H.Y., Oh, J.P., Kim, H.S., Kaang, B.K., et al. (2017). BAF53b, a Neuron-Specific Nucleosome Remodeling Factor, Is Induced after Learning and Facilitates Long-Term Memory Consolidation. J Neurosci 37, 3686-3697.
23. Bell, S., Maussion, G., Jefri, M., Peng, H., Theroux, J.F., Silveira, H., Soubannier, V., Wu, H., Hu, P., Galat, E., et al. (2018). Disruption of GRIN2B Impairs Differentiation in Human Neurons. Stem Cell Reports 11, 183-196.
24. Veres, A., Gosis, B.S., Ding, Q., Collins, R., Ragavendran, A., Brand, H., Erdin, S., Cowan, C.A., Talkowski, M.E., and Musunuru, K. (2014). Low incidence of off-target mutations in individual CRISPR-Cas9 and TALEN targeted human stem cell clones detected by whole-genome sequencing. Cell stem cell 15, 27-30.
25. Harada, A., Teng, J., Takei, Y., Oguchi, K., and Hirokawa, N. (2002). MAP2 is required for dendrite elongation, PKA anchoring in dendrites, and proper PKA signal transduction. The Journal of cell biology 158, 541-549.
26. Goedert, M., Crowther, R.A., and Garner, C.C. (1991). Molecular characterization of microtubule-associated proteins tau and MAP2. Trends Neurosci 14, 193-199.
27. Skjoerringe, T., Lundvig, D.M., Jensen, P.H., and Moos, T. (2006). P25alpha/Tubulin polymerization promoting protein expression by myelinating oligodendrocytes of the developing rat brain. J Neurochem 99, 333-342.
28. Mino, R.E., Rogers, S.L., Risinger, A.L., Rohena, C., Banerjee, S., and Bhat, M.A. (2016). Drosophila Ringmaker regulates microtubule stabilization and axonal extension during embryonic development. Journal of Cell Science 129, 3282-3294.
29. Kraft, R., Escobar, M.M., Narro, M.L., Kurtis, J.L., Efrat, A., Barnard, K., and Restifo, L.L. (2006). Phenotypes of Drosophila brain neurons in primary culture reveal a role for fascin in neurite shape and trajectory. J Neurosci 26, 8734-8747.
30. Stolt, C.C., Lommes, P., Friedrich, R.P., and Wegner, M. (2004). Transcription factors Sox8 and Sox10 perform non-equivalent roles during oligodendrocyte development despite functional redundancy. Development (Cambridge, England) 131, 2349-2358.
31. Boggs, J.M., Gao, W., Zhao, J., Park, H.J., Liu, Y., and Basu, A. (2010). Participation of galactosylceramide and sulfatide in glycosynapses between oligodendrocyte or myelin membranes. FEBS Lett 584, 1771-1778.
32. Kaczmarek, R., Mikolajewicz, K., Szymczak, K., Duk, M., Majorczyk, E., Krop-Watorek, A., Buczkowska, A., and Czerwinski, M. (2016). Evaluation of an amino acid residue

critical for the specificity and activity of human Gb3/CD77 synthase. Glycoconjugate Journal 33, 963-973.
33. Aref-Eshghi, E., Bend, E.G., Hood, R.L., Schenkel, L.C., Carere, D.A., Chakrabarti, R., Nagamani, S.C.S., Cheung, S.W., Campeau, P.M., Prasad, C., et al. (2018). BAFopathies' DNA methylation epi-signatures demonstrate diagnostic utility and functional continuum of Coffin–Siris and Nicolaides–Baraitser syndromes. Nature Communications 9, 4885.
34. Bogershausen, N., and Wollnik, B. (2018). Mutational Landscapes and Phenotypic Spectrum of SWI/SNF-Related Intellectual Disability Disorders. Front Mol Neurosci 11, 252.
35. Mari, F., Marozza, A., Mencarelli, M.A., Lo Rizzo, C., Fallerini, C., Dosa, L., Di Marco, C., Carignani, G., Baldassarri, M., Cianci, P., et al. (2015). Coffin-Siris and Nicolaides-Baraitser syndromes are a common well recognizable cause of intellectual disability. Brain and Development 37, 527-536.
36. Pretegiani, E., Mari, F., Renieri, A., Penco, S., and Dotti, M.T. (2016). Nicolaides-Baraitser syndrome: defining a phenotype. J Neurol 263, 1659-1660.
37. Kosho, T., Miyake, N., and Carey, J.C. (2014). Coffin-Siris syndrome and related disorders involving components of the BAF (mSWI/SNF) complex: historical review and recent advances using next generation sequencing. Am J Med Genet C Semin Med Genet 166c, 241-251.
38. Bender, H.A., Zaroff, C.M., Karantzoulis, S., Nakhutina, L., MacAllister, W.S., and Luciano, D. (2011). Cognitive and behavioral functioning in Coffin-Siris syndrome and epilepsy: a case presentation. The Journal of genetic psychology 172, 56-66.
39. Santen, G.W., Aten, E., Sun, Y., Almomani, R., Gilissen, C., Nielsen, M., Kant, S.G., Snoeck, I.N., Peeters, E.A., Hilhorst-Hofstee, Y., et al. (2012). Mutations in SWI/SNF chromatin remodeling complex gene ARID1B cause Coffin-Siris syndrome. Nat Genet 44, 379-380.
40. Vogel-Ciernia, A., and Wood, M.A. (2014). Neuron-specific chromatin remodeling: a missing link in epigenetic mechanisms underlying synaptic plasticity, memory, and intellectual disability disorders. Neuropharmacology 80, 18-27.
41. Wu, S., Shi, Y., Mulligan, P., Gay, F., Landry, J., Liu, H., Lu, J., Qi, H.H., Wang, W., Nickoloff, J.A., et al. (2007). A YY1-INO80 complex regulates genomic stability through homologous recombination-based repair. Nature structural & molecular biology 14, 1165-1172.
42. Vogel-Ciernia, A., Matheos, D.P., Barrett, R.M., Kramar, E.A., Azzawi, S., Chen, Y., Magnan, C.N., Zeller, M., Sylvain, A., Haettig, J., et al. (2013). The neuron-specific chromatin regulatory subunit BAF53b is necessary for synaptic plasticity and memory. Nat Neurosci 16, 552-561.
43. Laeremans, A., Van de Plas, B., Clerens, S., Van den Bergh, G., Arckens, L., and Hu, T.-T. (2013). Protein Expression Dynamics During Postnatal Mouse Brain Development. Journal of Experimental Neuroscience 7, 61-74.
44. Son, E.Y., and Crabtree, G.R. (2014). The role of BAF (mSWI/SNF) complexes in mammalian neural development. American journal of medical genetics Part C, Seminars in medical genetics 0, 333-349.

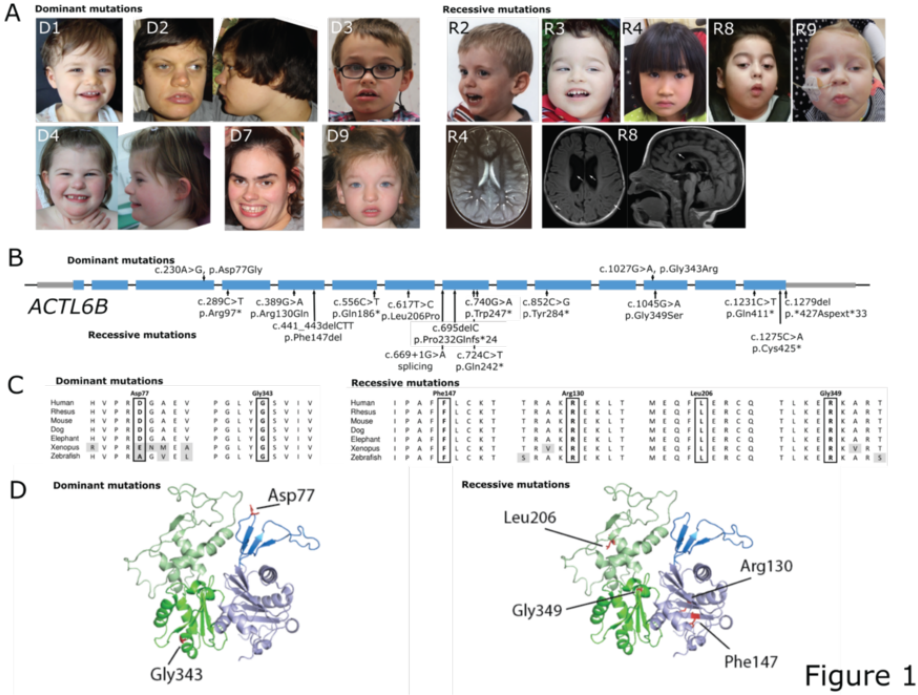
A
Dominant mutations
D1
D2
D3
D4
D7
D9
Recessive mutations
R2
R3
R4
R8
R9
R4
R8
B
Dominant mutations
c.230A>G, p.Asp77Gly
c.1027G>A, p.Gly343Arg
ACTL6B
c.289C>T p.Arg97*
c.389G>A p.Arg130Gln
c.441_443delCTT p.Phe147del
c.556C>T p.Gln186*
c.617T>C p.Leu206Pro
c.695delC p.Pro232Glnfs*24
c.669+1G>A splicing
c.724C>T p.Gln242*
c.740G>A p.Trp247*
c.852C>G p.Tyr284*
c.1045G>A p.Gly349Ser
c.1231C>T p.Gln411*
c.1279del p.*427Aspext*33
c.1275C>A p.Cys425*
Recessive mutations
C
Dominant mutations
Asp77
Gly343
Human H V P R D G A E V P G L Y G S V I V
Rhesus H V P R D G A E V P G L Y G S V I V
Mouse H V P R D G A E V P G L Y G S V I V
Dog H V P R D G A E V P G L Y G S V I V
Elephant H V P R D G A E V P G L Y G S V I V
Xenopus R V P R E N M E A P G L Y G S V I V
Zebrafish H V P R A G V E L P G L Y G S V I V
Recessive mutations
Phe147
Arg130
Leu206
Gly349
Human I P A F F L C K T T R A K R E K L T M E Q F L E R C Q T L K E R K A R T
Rhesus I P A F F L C K T T R A K R E K L T M E Q F L E R C Q T L K E R K A R T
Mouse I P A F F L C K T T R A K R E K L T M E Q F L E R C Q T L K E R K A R T
Dog I P A F F L C K T T R A K R E K L T M E Q F L E R C Q T L K E R K A R T
Elephant I P A F F L C K T T R A K R E K L T M E Q F L E R C Q T L K E R K A R T
Xenopus I P A F F L C K T T R V K R E K L T M E Q F L E R C Q T L K E R K V R T
Zebrafish I P A F F L C K T S R A K R E K L T M E Q F L E R C Q T L K E R K A R S
D
Dominant mutations
Asp77
Gly343
Recessive mutations
Leu206
Arg130
Gly349
Phe147

Figure 1

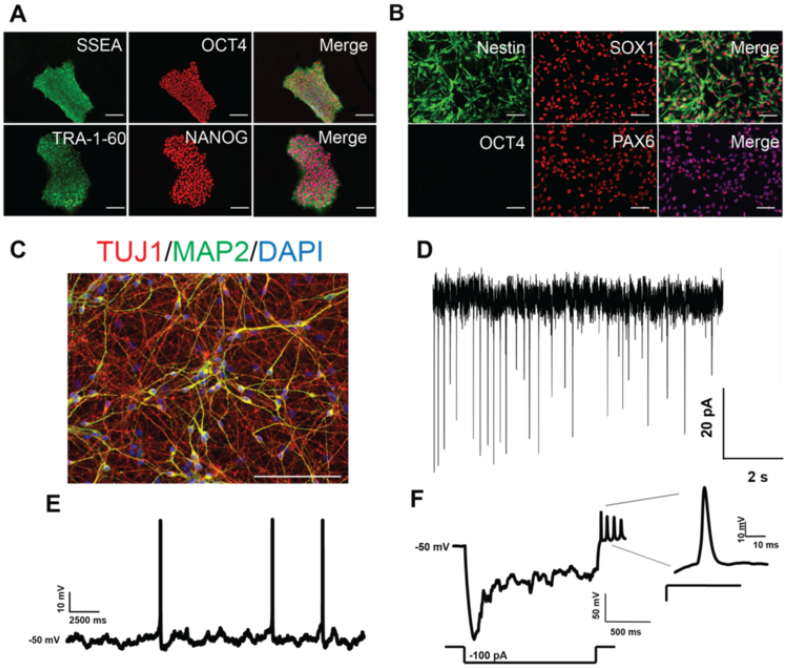
A
SSEA
OCT4
Merge
TRA-1-60
NANOG
Merge
B
Nestin
SOX1
Merge
OCT4
PAX6
Merge
C
TUJ1/MAP2/DAPI
D
20 pA
2 s
E
10 mV
2500 ms
-50 mV
F
-50 mV
50 mV
500 ms
-100 pA
10 mV
10 ms

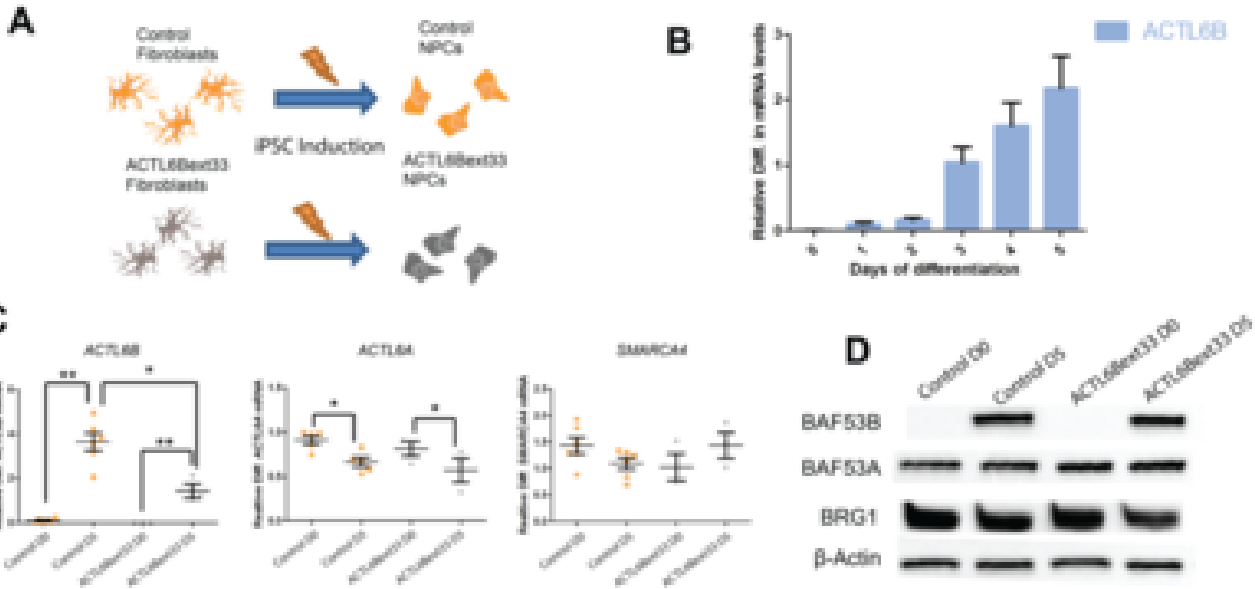
A
Control Fibroblasts
iPSC Induction
Control NPCs
ACTL6Bext33 Fibroblasts
ACTL6Bext33 NPCs
B
ACTL6B
Relative Diff. in mRNA levels
Days of differentiation
C
ACTL6B
ACTL6A
SMARCA4
D
Control D0
Control D5
ACTL6Bext33 D0
ACTL6Bext33 D5
BAF53B
BAF53A
BRG1
β-Actin

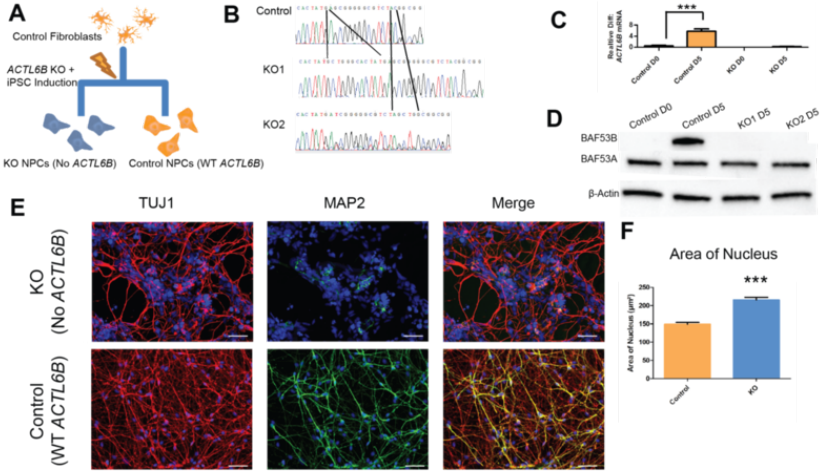
A
Control Fibroblasts
ACTL6B KO + iPSC Induction
KO NPCs (No ACTL6B)
Control NPCs (WT ACTL6B)
B
Control
KO1
KO2
C
***
Control D0
Control D5
KO1 D5
KO2 D5
D
Control D0
Control D5
KO1 D5
KO2 D5
BAF53B
BAF53A
β-Actin
E
TUJ1
MAP2
Merge
KO (No ACTL6B)
Control (WT ACTL6B)
F
Area of Nucleus
***
Control
KO

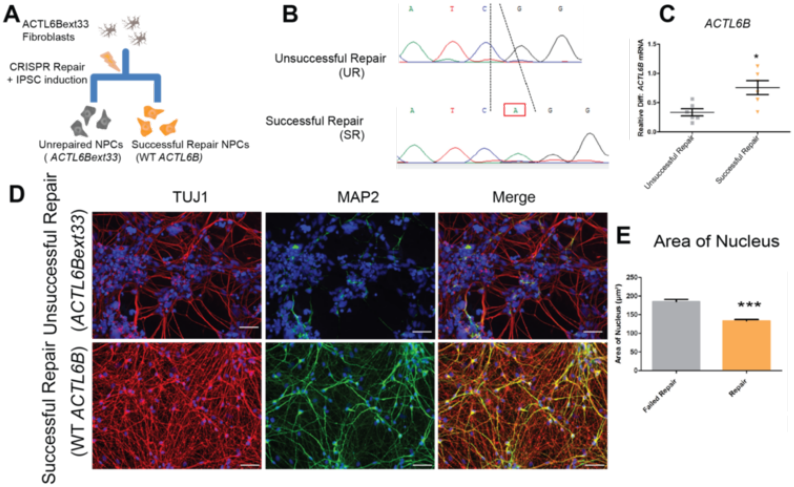
A
ACTL6Bext33
Fibroblasts
CRISPR Repair
+ IPSC induction
Unrepaired NPCs
(ACTL6Bext33)
Successful Repair NPCs
(WT ACTL6B)
B
Unsuccessful Repair
(UR)
Successful Repair
(SR)
C
ACTL6B
Relative Diff. ACTL6B mRNA
Unsuccessful Repair
Successful Repair
D
TUJ1
MAP2
Merge
Successful Repair (WT ACTL6B)
Unsuccessful Repair (ACTL6Bext33)
E
Area of Nucleus
Area of Nucleus (µm²)
***
Failed Repair
Repair


A
Control NPCs
ACTL6Bext33 NPCs
Crosslink protein and DNA (DO and D5 cells)
Add Antibodies Reverse Crosslink
ChIP Sequencing

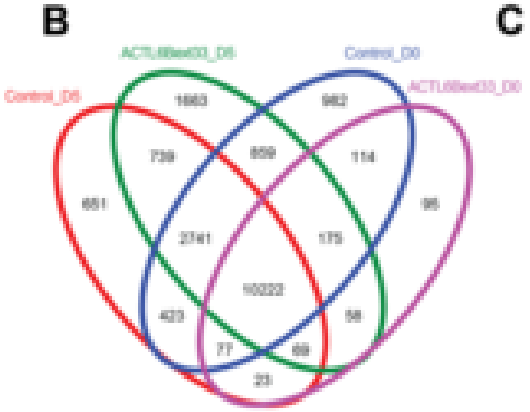
B
ACTL6Bext33_D5
Control_D0
Control_D5
ACTL6Bext33_D0
1663
982
739
899
114
651
95
2741
175
10222
423
58
77
69
23

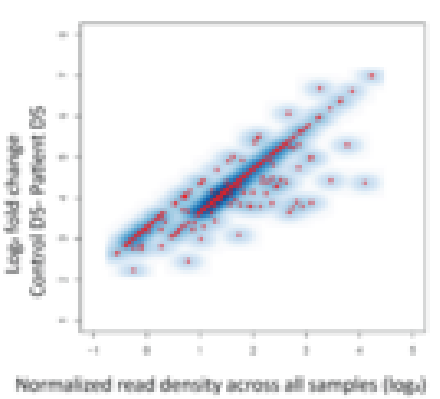
C
Log2 fold change Control D5- Patient D5
Normalized read density across all samples (log2)

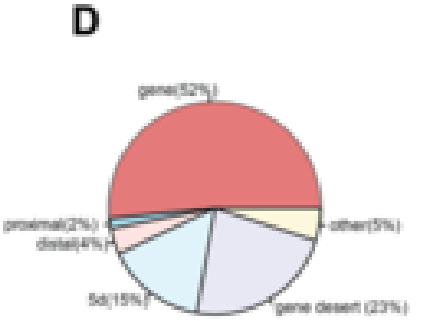
D
gene(52%)
other(5%)
distal(4%)
proximal(2%)
5d(15%)
gene desert (23%)

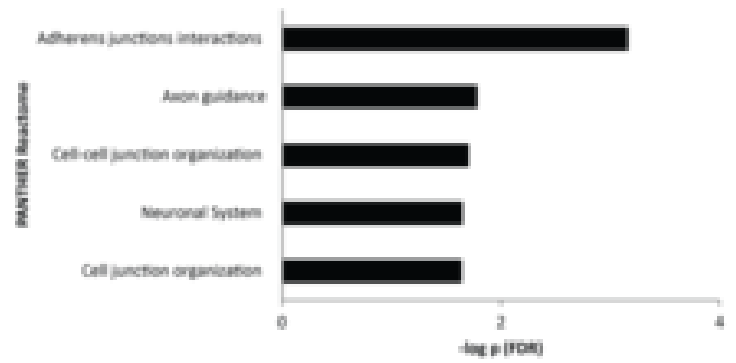
E
Adherens junctions interactions
Axon guidance
Cell-cell junction organization
Neuronal System
Cell junction organization
REACTOME Reactome
0
2
4
-log p (FDR)

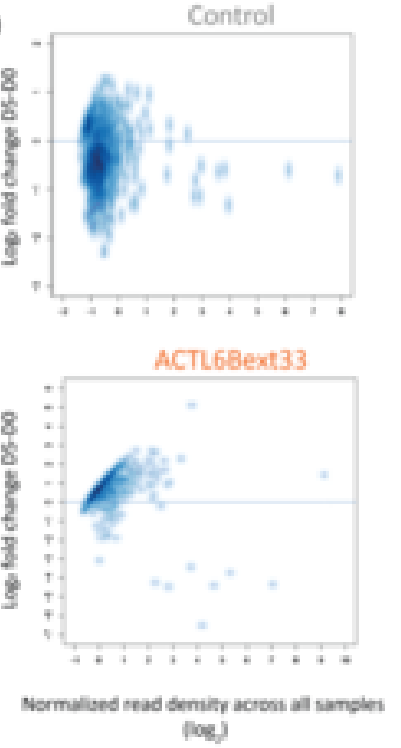
F
Control
ACTL6Bext33
Log2 fold change D5-D0
Normalized read density across all samples (log2)

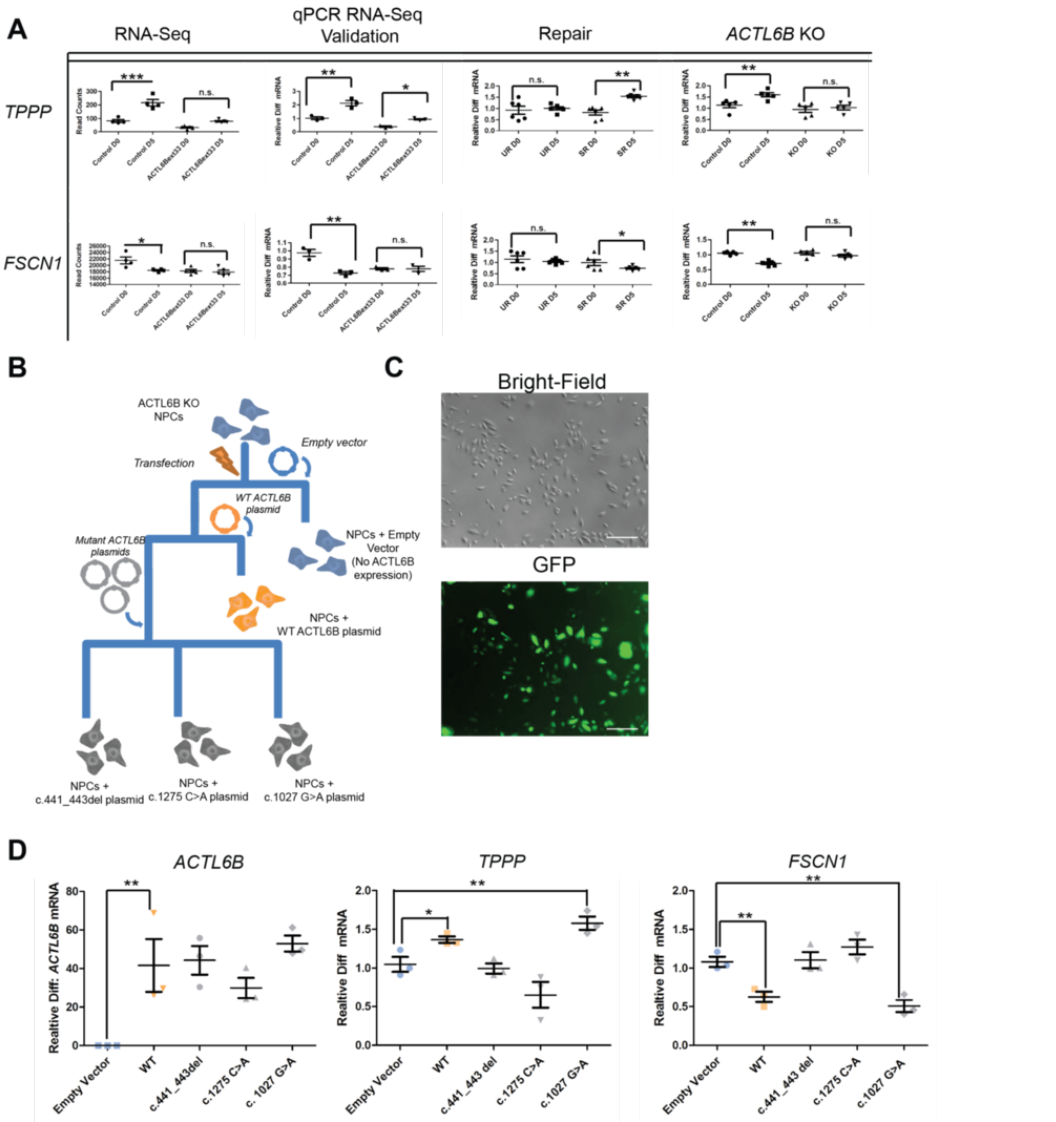
A
RNA-Seq
qPCR RNA-Seq Validation
Repair
ACTL6B KO
TPPP
FSCN1
Read Counts
Realtive Diff mRNA
Control D0
Control D5
ACTL6Bex333 D0
ACTL6Bex333 D5
UR D0
UR D5
SR D0
SR D5
KO D0
KO D5
n.s.
B
ACTL6B KO NPCs
Transfection
Empty vector
WT ACTL6B plasmid
Mutant ACTL6B plasmids
NPCs + Empty Vector (No ACTL6B expression)
NPCs + WT ACTL6B plasmid
NPCs + c.441_443del plasmid
NPCs + c.1275 C>A plasmid
NPCs + c.1027 G>A plasmid
C
Bright-Field
GFP
D
ACTL6B
TPPP
FSCN1
Realtive Diff: ACTL6B mRNA
Realtive Diff mRNA
Empty Vector
WT
c.441_443del
c.1275 C>A
c. 1027 G>A

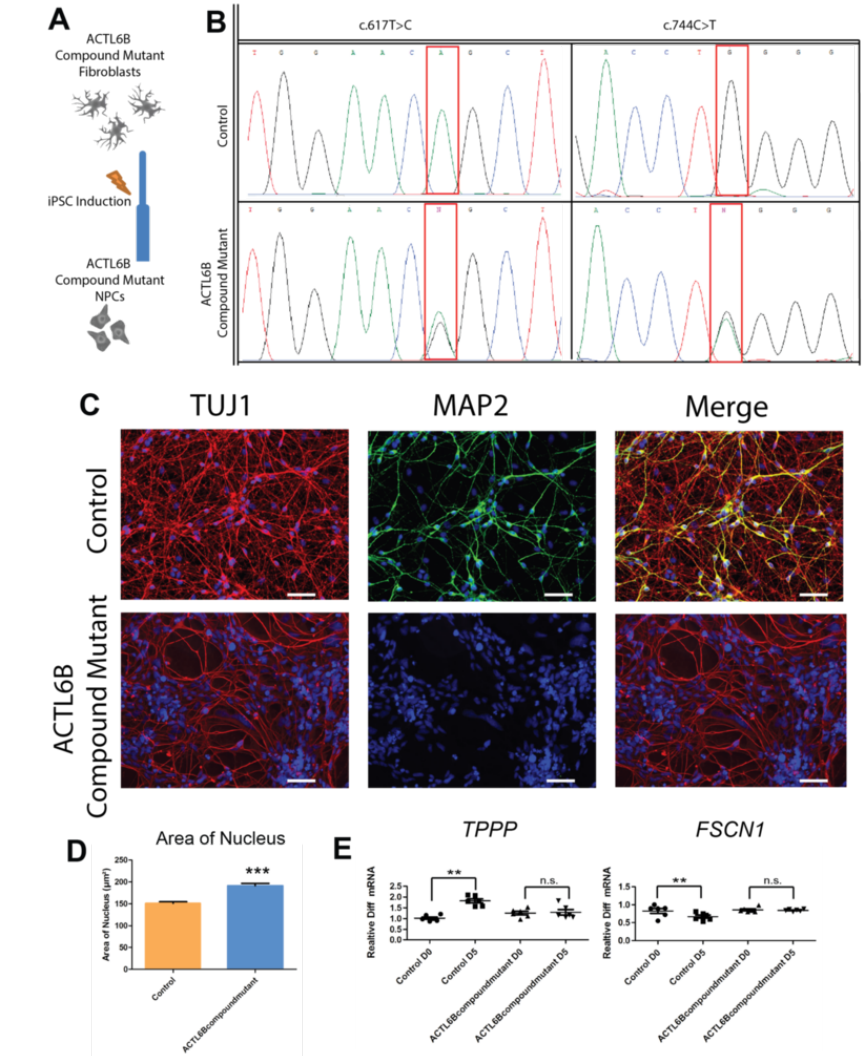
A
ACTL6B
Compound Mutant
Fibroblasts
iPSC Induction
ACTL6B
Compound Mutant
NPCs
B
c.617T>C
c.744C>T
Control
ACTL6B
Compound Mutant
C
TUJ1
MAP2
Merge
Control
ACTL6B
Compound Mutant
D
Area of Nucleus
Area of Nucleus (μm²)
***
Control
ACTL6BcompoundMutant
E
TPPP
FSCN1
Realtive Diff mRNA
**
n.s.
Control D0
Control D5
ACTL6BcompoundMutant D0
ACTL6BcompoundMutant D5